Geometrical Invariance and Smoothness Maximization for Task-Space Movement Generation

Article *in* IEEE Transactions on Robotics · July 2016

DOI: 10.1109/TRO.2016.2581208

3 authors, including:

Yaron Meirovitch
Harvard University
41 PUBLICATIONS **703** CITATIONS
SEE PROFILE

Tamar Flash
Weizmann Institute of Science
220 PUBLICATIONS **14,740** CITATIONS
SEE PROFILE

Geometrical Invariance and Smoothness Maximization for Task-Space Movement Generation

Yaron Meirovitch, Daniel Bennequin, and Tamar Flash

***Abstract*—In human motor control studies, end-effector (e.g., hand) trajectories have been successfully modeled using optimization principles. Yet, it remains unclear how such trajectories are updated when the end-effector or task goals are perturbed. Here, we present an approach to human and robotic task-level trajectory planning and modification using geometrical invariance and optimization, allowing to adapt learned movements to *a priori* unknown boundary conditions. The optimization criterion represents a tradeoff between smoothness (minimum jerk) and accuracy (jerk–accuracy model). We show that planning maximally smooth movements allows recovery from perturbations by superimposing specific affine orbits on maximally smooth preplanned trajectories. The generated trajectories are compared with those resulting from other recent approaches used in robotics. Finally, we discuss conditions for affine invariance of maximally smooth task-space trajectories. Possible applications of this study to both human motor control and robotics research studies are discussed.**

***Index Terms*—Invariance, kinematics, motion control, optimization, path planning for manipulators.**

I. Introduction

WHAT computational mechanisms allow humans to produce stereotypical movements under environmental uncertainties? Several lines of research suggested that feedback mechanisms implemented by sensory-motor loops within the central nervous system (CNS) allow swift adaptation to new task requirements. However, how movement corrections are smoothly integrated into the trajectory plan is not fully understood. Also not well understood is how humans achieve a variety of motor goals in the presence of long delays in processing sensory feedback [1]. Finally, albeit recent progress in the understanding of human movement invariance [2], it remains a mystery how complex movements are effortlessly produced in a stereotypical manner.

Various approaches to the modeling of upper arm and locomotion trajectories have been developed. One prominent approach is that of optimal control assuming different cost functions such as smoothness maximization by minimizing jerk [3]–[5], acceleration [6], or related kinematic costs [7]. Other models have used dynamic costs such as the minimization of energy [8], [9], rate of change of torque [10], or movement variance in the presence of signal-dependent noise [11]. A more recently developed optimal feedback control model has emphasized the importance of feedback while questioning the existence of the preplanning of desired trajectories by the brain [12]. The development of optimization-based approaches have also played an important role in motion planning for robotic systems, whereas the most prevailing approach involved separating the problem into two different subproblems: the first addressing the path planning task, while the second dealing with trajectory tracking—executing trajectories that track the preplanned spatial paths.

In human motor control, it is unclear whether there exists a separation between path planning and detailed specification of time-dependent trajectory profiles (but see [9]). A prevasive dependence between path geometry and velocity, however, has long been established [13]. For point-to-point movements, the path of the end-effector is roughly straight, and the velocity profile is bell shaped and is invariant to temporal and spatial scaling required to accomplish the motor task [3]. Evidence for strong coupling between path curvature and end-effector velocity was repeatedly provided, mathematically captured by the 2/3 [14] and related power laws [2], [15]–[17].

The stereotypical nature of human movements and the ability of humans to rapidly adapt their movements may arise from neural encoding of the spatial and temporal regularities characterizing human movement generation (MG) [18]. Recent brain mapping (fMRI and EEG) studies suggest the existence of neural representations of movement regularities that could simplify the complex computations required for both motor production and perception [19], [20]. These findings may imply the existence of internal models that afford such capabilities [1], [18].

The above findings are potentially of great significance to humanoid robotics research. A considerable number of studies in robotics have adopted similar optimization principles to those used in modeling human movement, such as jerk minimization of robot manipulators' end-effectors (e.g., [21]) or maximizing the smoothness of center of mass trajectories [7], during humanoid locomotion [22]. Similar approaches have also inspired the development of motion planning algorithms for robot reaching, writing, obstacle avoidance, etc. Moreover, as robotics research aims at enhancing human–robot interaction, by adopting motion planning strategies that are compatible with human motor control strategies, greater compatibility, easier and more flexible modes of operation of robotic systems will allow faster

Manuscript received February 01, 2016; revised May 31, 2016; accepted June 02, 2016. This paper was recommended for publication by Editor A. Kheddar upon evaluation of the reviewers' comments. This work was supported by Koroibot FP7-ICT-2013-10/ 611909, AMARSi FP7-ICT-248311, and ICORE ISF.

Y. Meirovitch is with the Computer Science and Artificial Intelligence Laboratory, Massachusetts Institute of Technology, Cambridge, MA 02139 USA (e-mail: yaronm@csail.mit.edu).

D. Bennequin is with Paris Diderot University, 75013 Paris, France (e-mail: bennequin@math.jussieu.fr).

T. Flash is with the Department of Computer Science and Applied Mathematics, Weizmann Institute of Science, Rehovot 7610001, Israel (e-mail: tamar.flash@weizmann.ac.il).

Color versions of one or more of the figures in this paper are available online at http://ieeexplore.ieee.org.

Digital Object Identifier 10.1109/TRO.2016.2581208

and more successful use of robots in different tasks such as rehabilitation [23], taking care of the elderly, and service robotics [24].

Another influential notion shared between research in human motor control and robotics is that of motion primitives—the idea that complex movements are constructed from elementary building blocks or simpler motion templates. Using motion templates and applying different geometrical and temporal transformations to such primitives, and then ordering and stringing them together into sequential tasks, is a computationally efficient mechanism for constructing multiple behaviors from a small number of motor primitives. While the tendency is to *a priori* assume using motions that are invariant under Euclidean transformations, recent studies have indicated that motion primitives in human and primate movements are invariant under equiaffine [25], [26] or under a mixture of Euclidean, affine, and equiaffine transformations [2].

Motivated by the prevalence of affine invariance in human action and perception, Pham and Nakamura developed a motion generation algorithm that applies affine deformations to a preplanned end-effector trajectory in order to deal with unexpected perturbations. In their work, Pham and Nakamura explain that the deformed trajectory preserves the affine-invariant features of the original trajectory such as smoothness and affine velocity [27]. Complementing their study, we develop here algorithms that conjugate affine transformations and smoothness optimization. Notably, the optimization used here to formulate end-effector trajectories (jerk–accuracy (JA) model) is affine invariant.

The study presented here focuses on human and robotic task-level trajectory planning. Unlike other approaches developed in robotics, the approach taken here does not separate between path and trajectory planning. Instead, we present, here, a particular approach to the modeling of human trajectories, suggesting that the motor system plans movements that maximize smoothness—expressed by the minimization of a kinematic cost that depends on higher order time derivatives of position (e.g., acceleration, jerk, or even snap), the so-called mean-squared derivative (MSD) cost. Although smooth functions are traditionally referred to as functions infinitely differentiable, motor control studies have used MSD costs in order to assess the degree of smoothness of the trajectory of a point moving along some path as a function of time. The notion of smoothness depends on the order of the time derivative used by the MSD cost. Depending on the motor task being studied, it was found that jerk minimization ($n = 3$) better applies to hand trajectories [3], while a model involving the minimization of acceleration of the center of mass trajectory ($n = 2$) was found to provide a better model for human locomotion [22].

The movements produced by the suggested approach are shown to be a superposition of a maximally smooth template trajectory (a potential motor plan) with a series of affine orbits (optimal correction terms). The simplicity of the solution is used to devise a real-time MG algorithm that is capable of producing stereotypical movements, while overcoming perturbations in task space. The performance of our MG algorithm is tested here by regenerating previously recorded hand movements and simulating various perturbations applied to the generated end-effector trajectories [28].

Previous research in robotics suggested parameterizing task- and joint-space trajectories using different building blocks, notably dynamic movement primitives (DMPs) [29], [30] and Gaussian mixture models. Although approaches such as DMPs offer equally smooth and accurate trajectory reproduction in the case of perturbations, here we make no assumption about the parameterization of the desired or regenerated trajectories. We also do not look at the optimization of torques and forces to be used by humans or robots for achieving the predicted end-effector trajectory. Instead, we directly derive the trajectory by minimizing a weighted sum composed of the L^2 norm of the jerk profile [3] ("smoothness") and the L^2 norm of the time-dependent distance from the desired template ("error"). We later show that an arbitrarily complex movement can be parameterized by a set of polynomials (in effect of any degree) and solve for the maximally smooth regeneration of these polynomials.

A. Organization of the Paper

The paper is organized as follows. In Section II, we present new theoretical results concerning the organizing geometric principles and the precise temporal predictions of frequently used models for end-effector's smoothness maximization in point-to-point, via-point, and path-constrained movements. In Section III, we propose the JA model and an algorithm for optimal, adaptive, and stable regeneration of arbitrary task-space trajectories, satisfying arbitrary boundary conditions. In Section IV, we discuss a new notion of affine invariance for maximally smooth unconstrained movements, movements through via-points, path-constrained movements, and the new JA model. In Section V, we devise a real-time implementation of the JA MG algorithm and compare its performance with that of recent approaches in robotics, using a recent robotics benchmark system, which simulates perturbations and evaluates different robotics MG algorithms that learn from few human demonstrations [28]. In Section VI, we discuss our MG algorithm and the potential of defining movement complexity through optimization criteria, such as the minimum jerk model [3], and based on geometrical invariance (which we introduced in the context of motor control in [2] and [25]).

II. Modeling Movement Based on Maximizing Smoothness

We consider in this section an assumption derived from the above notion of movement primitives [31], [32], namely that temporal ordering is required for the planning and representation of complex motor tasks. A large part of the presented results are relevant for robotic motion generation and human–robot interaction. In particular, certain kinematic and temporal features of human movements, as expressed by Fitts' law [33] and the derivation of constants of motion (see Section II-E), can be useful for robotic applications involving human–robot interactions to ensure compatibility between human and robot behaviors. These characteristics can also be used to assess the human likeness of robot movements.

The smoothness of a task-space trajectory $\boldsymbol{r}$ is defined in the paper by an MSD model of order n

$$\int_0^T \left| \frac{d^n}{dt^n} \boldsymbol{r} \right|^2 dt. \tag{1}$$

Minimizing (1) for $n = 3$ was termed the "minimum jerk model" [34].

The minimum jerk model: The smoothness maximization principle was frequently expressed as the minimization of the mean-squared norm of the time derivative of acceleration, i.e., jerk, expressed in terms of end-effector coordinates [3]

$$\min I_T(\boldsymbol{r}) \quad \text{subject to } \boldsymbol{B}$$
$$I_T(\boldsymbol{r}) = \int_0^T L(t, \boldsymbol{r}, \dot{\boldsymbol{r}}, \ddot{\boldsymbol{r}}, \dddot{\boldsymbol{r}}) dt \tag{2}$$

with the Lagrangian $L(t, \boldsymbol{r}, \dot{\boldsymbol{r}}, \ddot{\boldsymbol{r}}, \dddot{\boldsymbol{r}}) = \dddot{\boldsymbol{r}} \cdot \dddot{\boldsymbol{r}}$, where $\boldsymbol{r}(t) : [0, T] \to \mathbb{E}^d$ is the end-effector trajectory expressed in the Euclidean space $\mathbb{E}^d$; the upper dots represent derivatives with respect to time; the $\cdot$ notation represents the inner-product in $\mathbb{E}^d$; T is the duration of the movement; and $\boldsymbol{B}$ is a set of task-dependent constraints (e.g., boundary conditions). The Lagrangian L depends on the inner product in $\mathbb{E}^d$ and does not depend on the choice of vector space coordinates. Therefore, (2) is a Euclidean cost (in Section IV, we discuss the properties of this model with respect to Euclidean and affine invariance).

A. Point-to-Point Jerk Minimization

A special choice of boundary conditions $\boldsymbol{B}$ could consist of fixed endpoint positions, for which the velocities and accelerations are zero. This was shown to predict the straightness and the bell-shaped velocity profiles of human point-to-point movement [3]. In general, for any fixed endpoint positions, velocities and accelerations the Euler–Lagrange (EL) equation is

$$\boldsymbol{r}^{(6)} \equiv 0 \tag{3}$$

where $^{(k)}$ represents the kth-order time derivative of the task-space trajectory.

B. Point-to-Point Mean-Squared Derivative Minimization

Alternatively, it has been suggested that rapid arm movements are better represented using a minimum acceleration model and assuming lower and upper bounds that constrain the jerk profile [6]. According to optimal control theory, the optimization of this minimum acceleration model results in a segmentwise constant jerk profile. Other studies suggested that locomotion paths are better described by minimum acceleration trajectories, including a cost associated with body orientation rather than jerk [22]. Different notions of smoothness were also considered by minimizing the nth-order time derivative of position, as in (1), subject to boundary conditions $\boldsymbol{B}$.

The extremals of such MSD cost functions satisfy the equation [35]

$$\boldsymbol{r}^{(2n)} \equiv 0 \tag{4}$$

which generalizes (3) to a differentiation order of n [15]. Equation (4) is often used to predict end-effector trajectories by assuming fixed boundary conditions or by minimizing (1) with variable boundary conditions [36], [37]. Later, Svinin, Goncharenko, Luo, and Hosoe generalized the solution (4) to the case of a real number n, using a regularized incomplete Beta function [36].

Solutions to (4) are $(2n-1)$-order time-dependent polynomials whose coefficients are linear functions of the assumed boundary conditions. For optimal trajectories with vanishing $(n-1)$-order time derivatives at the endpoints, the total MSD cost, denoted by A_n [(1) and (4)], depends quadratically on the amplitude of the straight trajectory, L, and inversely on the $(2n-1)$ power of the duration T of the movement

$$A_n = f(n) \frac{L^2}{T^{2n-1}} \tag{5}$$

where $f(n)$ is a coefficient that depends only on the order of differentiation n, and the amplitude L is the Euclidean distance between the trajectory endpoints [see Appendix C]. It has been shown that increasing the differentiation order n does not improve the accuracy of fit to human movement, whereas for larger ns, the larger number of polynomial coefficients requires the specification of a larger number of boundary conditions [15]. Equation (5) is later combined with Fitts' law to associate the cost of smoothness with the accuracy demands at the endpoint.

The linear combination of MSD cost functions (1) of different differentiation orders n results in a superposition of the solution to the MSD cost function (4) with a nonpolynomial component. For example, the cost functional

$$\int_0^T \omega_1 \left| \dddot{\boldsymbol{r}}(t) \right|^2 + \omega_2 \left| \ddot{\boldsymbol{r}}(t) \right|^2 dt \tag{6}$$

is a linear combination of a minimum jerk $(n = 3)$ and a minimum acceleration $(n = 2)$ cost whose minima satisfy

$$\left(\omega_1 \frac{d^6}{dt^6} + \omega_2 \frac{d^4}{dt^4} \right) \boldsymbol{r}(t) \equiv 0. \tag{7}$$

The solution of (7) in the plane (i.e., $d = 2$) for positive ω_1 and ω_2 is the superposition of a solution to (4) for $n = 2$ and an elliptical trajectory

$$\boldsymbol{r}_{\text{opt}} = \boldsymbol{A} \begin{pmatrix} \cos \theta t \\ \sin \theta t \end{pmatrix} + \boldsymbol{p}(t) \tag{8}$$

where $\theta = (\omega_2/\omega_1)^{1/2}$, the matrix $\boldsymbol{A} \in \mathbb{R}^{2\times 2}$ represents a linear transformation, and $\boldsymbol{p}(t)$ is a 2-D third order time polynomial. The relative weight ω_2/ω_1 of the minimum acceleration component in (6) is quadratically related to the frequency of the oscillations of the elliptical component in (8). We note that the fourth- and fifth-order terms of the unconstrained minimum jerk solution do not exist in the combined acceleration-jerk cost, which are, in turn, substituted by an elliptical movement path.

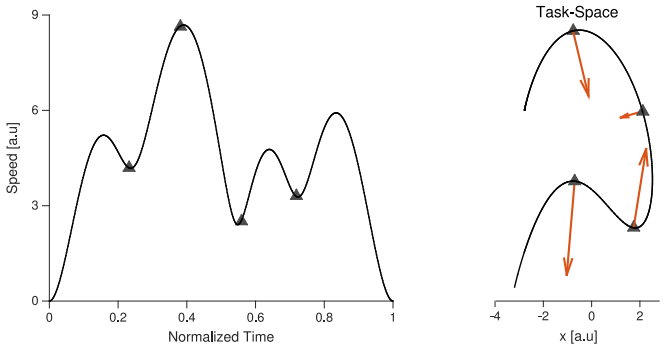

Fig. 1. Minimal jerk via-point trajectory. Via-points are marked by triangles. (Right): Differences between the fifth-order time derivatives computed before and after the via-points are marked by arrows (right panel) and are shown to be perpendicular to the tangent to the path as predicted by (9). Via-points nearly coincide with the curvature extrema, which is characteristic of the minimal jerk via-point problem. (Left): Speed at via-points approximately reaches an extremum.

This example shows that a linear combination of costs of different orders results in a complex solution, which is not an obvious manipulation of the optimal solutions to the individual costs. The solution to this jerk-acceleration cost predicts an oscillatory component, which also appears later in our solution to the JA tradeoff (see Section III).

C. Movements Through Internal Via-Points

In this case, the motor task is defined by an additional constraint that the movement should pass through an intermediate via-point, $\boldsymbol{c_0}$. Unlike the tendency in motor control and robotics research to assume the exact time of passage through the via-points, here, as in [3], these times are predicted from MSD optimization.

It was shown that for the optimal trajectory minimizing (2), $\boldsymbol{r}(t)$ must satisfy (3) for all t such that $\boldsymbol{r}(t) \neq \boldsymbol{c_0}$ and be fourth-order differentiable (all derivatives up to the fourth order are continuous) at the via-point and

$$\left(\boldsymbol{r}_+^{(5)}(t_1) - \boldsymbol{r}_-^{(5)}(t_1)\right) \cdot \dot{\boldsymbol{r}}(t_1) = 0$$
$$\boldsymbol{r}(t_1) = \boldsymbol{c_0} \tag{9}$$

for some $0 \leq t_1 \leq T$, where $\cdot$ is the inner product in $\mathbb{E}^d$ [3], [38]. In Euclidean terms, according to (9), the difference between the fifth-order time derivatives before and after $\boldsymbol{c_0}$ is perpendicular to the tangent to the curve. Since the trajectories before and after the via-point must satisfy (3), one can confirm that the number of constraints, including the boundary conditions, the continuity at the via-point, and (9), is equal to the number of coefficients defining the polynomials before and after the via-point. By the same argument, this readily generalizes to an arbitrary number of task-space via-points [3], [38] (see Fig. 1). Thus, the via-point optimization (10) is completely characterized by (9) and the above continuity conditions. Further, it extends to a general differentiation order n and to a general dimension d, as defined by the MSD model (1) [35], by satisfying (4) and additionally that the optimal trajectory is $(2n-2)$-order differentiable at the via-point and

$$\left(\boldsymbol{r}_+^{(2n-1)}(t_1) - \boldsymbol{r}_-^{(2n-1)}(t_1)\right) \cdot \dot{\boldsymbol{r}}(t_1) = 0$$
$$\boldsymbol{r}(t_1) = \boldsymbol{c_0}. \tag{10}$$

Fig. 1 shows an example of a via-point optimal trajectory $(n = 3)$, where the differences between the fifth-order time derivatives of consecutive segments were numerically calculated and drawn at the via-points (right panel). These differences are indeed perpendicular to the tangents to the trajectories at the via-points as dictated by (10). The speeds and curvatures at the via-points nearly coincide with speed extrema and curvature maxima, respectively.

D. Path-Constrained Movements

The constrained minimum jerk model [4] was shown to successfully predict the kinematics of drawing movements [4], [15] and locomotion [2]. The model assumes a path constraint $\boldsymbol{r}(\zeta) \in \mathbb{E}^d$, where ζ is an arbitrary parameterization and predicts the minimization of (2) over all possible time-parameterizations $\zeta(t)$

$$\min_{\zeta(t)} I_T(\boldsymbol{r}(\zeta)) \quad \text{subject to } \boldsymbol{B}. \tag{11}$$

We prove (see Appendix A) that the minimization (11) is equivalent to the equation

$$\boldsymbol{r}^{(6)}(\zeta) \cdot \dot{\boldsymbol{r}}(\zeta) = 0 \quad \forall \zeta \tag{12}$$

where the derivatives are taken with respect to time. The time parameterization $\zeta(t)$ solving (12) is an extremum of the jerk functional. Equation (12) generalizes [26], which proved a similar equation for the restricted case of equiaffine parameterization. From a geometrical point of view for any constrained minimum jerk trajectory, (12) predicts that the sixth-order time derivative of the trajectory lies in the direction of the normal to the curve [cf., (9)]. This readily extends to a general MSD optimization problem [see (1) and (11)], where the extremals are characterized by the equation

$$\boldsymbol{r}^{(2n)}(\zeta) \cdot \dot{\boldsymbol{r}}(\zeta) \equiv 0. \tag{13}$$

This Euclidean equation states that for path-constrained optimal n-order MSD, the $2n$-order time derivative is perpendicular to the tangent to the path. Equation (13) applies also to the path-constrained problem in 3-D space (i.e., $d = 3$).

E. Constants of Motion

Here, we derive a set of local quantities that characterize maximally smooth trajectories and are independent of the coordinate frame used to represent the trajectory. Our derivation suggests that optimal ("human-like") trajectories can be identified in real time by quantifying the divergence of a recorded movement from optimality, which can be beneficial to a human–robot application whereby the human likeness of task-space trajectories is continuously assessed (e.g., for tracking a human agent) as well as for human–robot application for which human likeness of trajectories needs to be determined in real time.

1) Constants of Unconstrained Minimum Jerk Movements: A set of time-independent constants of motion can be determined by integration of the EL equations. For example, integrating (4)

$$\int \boldsymbol{r}^{(2n)}(t)dt \equiv \boldsymbol{\gamma} \in \text{task space} \tag{14}$$

results in a constant of motion that depends on the fixed Euclidean frame and is independent of the time axis. Thus, for minimal jerk point-to-point trajectories ($n = 3$), the fifth-order time derivative of the trajectory is a constant of motion, whose norm is a Euclidean invariant.

To form other Euclidean invariant time-independent constants of motion, we directly integrate the inner products

$$G_k^n(t) := \int \boldsymbol{r}^{(k)} \cdot \boldsymbol{r}^{(2n)} dt.$$

Due to (4), the integrand vanishes for any integer k, and we obtain $G_k^n(t) \equiv$ Const. Hence, by integration by parts, we get for $n = 3$

$$G_k^3(t) = \begin{cases} \dfrac{1}{2}\boldsymbol{r}^{(5)} \cdot \boldsymbol{r}^{(5)}, & k = 5 \\ \boldsymbol{r}^{(3)} \cdot \boldsymbol{r}^{(5)} - \dfrac{1}{2}\boldsymbol{r}^{(4)} \cdot \boldsymbol{r}^{(4)}, & k = 3 \\ \boldsymbol{r}^{(1)} \cdot \boldsymbol{r}^{(5)} - \boldsymbol{r}^{(2)} \cdot \boldsymbol{r}^{(4)} + \dfrac{1}{2}\boldsymbol{r}^{(3)} \cdot \boldsymbol{r}^{(3)}, & k = 1. \end{cases} \tag{15}$$

For brevity, we omitted the time dependences of $\boldsymbol{r}$ and its derivatives on t from the right-hand side (RHS) of these identities. The last constant ($k = 1$) has been studied in the context of jerk minimization and equiaffine geometry [26] and recently by Huh in the context of unconstrained minimum jerk and the hypothesis of constant drive [39]. We denote by D_3 this constant drive $D_3 = G_1^3$.

These constants of motion are local characteristics of unconstrained minimal jerk trajectories ($n = 3$), which readily generalizes to an arbitrary MSD order n. Later, we will use these constants to predict the total durations of maximally smooth movements.

2) Constants of Path-Constrained Minimum Jerk Movements: Above, we discussed the path-constrained minimum jerk model [4] and presented (12), which characterizes optimal solutions. We can use (12) to prove that the constant of motion G_1^3 in (15) also holds for path-constrained minimal jerk trajectories

$$\boldsymbol{r}^{(1)} \cdot \boldsymbol{r}^{(5)} - 2\boldsymbol{r}^{(2)} \cdot \boldsymbol{r}^{(4)} + \boldsymbol{r}^{(3)} \cdot \boldsymbol{r}^{(3)} \equiv D_3 \tag{16}$$

where the constant $D_3 = G_1^3$ is derived from integrating (12). Equation (16) is, therefore, the counterpart of the point-to-point time invariant fifth-order time derivative (14).

3) Constants of Via-Point Minimum Jerk Movements: The constant of motion described above for unconstrained and path-constrained jerk minimization, D_3, also holds for the optimal segments of the via-point solution. However, it is not clear *a priori* what the relationships are between the constants of motion of different segments. We prove that for via-point optimization, the constant D_3^- before the via-point is equal to the constant D_3^+ after the via-point, which is a consequence of (9) (see Appendix B)

$$D_3^i = D_3^j \quad \forall ij. \tag{17}$$

This property can thus be used to assess the appropriateness of using a single smoothness optimization to model an entire complex movement, which could otherwise be conjectured to be composed of several independent optimal trajectories. Similar properties of continuities of constants of motion can also be derived for other MSD optimization problems with via-point constraints.

F. Analytically Deriving the Total Duration From the Local Kinematics

We now show how to replace the global requirement of a prescribed total duration T with a local kinematic requirement. For zero velocities and accelerations at the boundaries, the unconstrained minimum jerk model predicts a straight trajectory and the total duration T from the initial conditions as well as from the constants of motion (see Section II-E) along the trajectory

$$T = \sqrt[3]{\frac{60L}{\left|\dddot{\boldsymbol{r}}(0)\right|}} = \sqrt[5]{\frac{6!L}{\left|\boldsymbol{r}^{(5)}(t)\right|}} \quad \forall t \tag{18}$$

where the extent of the straight movement, L, is the Euclidean distance between the trajectory endpoints. The equations in (18) map the initial jerk and the magnitude of the fifth-order time derivatives of the trajectories to their movement duration. The total duration can also be linked to global costs, e.g., the total accumulated acceleration or jerk by

$$T = \sqrt[3]{\frac{5!L^2}{7A_2}} = \sqrt[5]{\frac{6!L^2}{A_3}} \tag{19}$$

where the total acceleration and the total jerk, A_2 and A_3, are defined as in (1), respectively.

This approach can be applied to predict movement duration in the context of a general MSD model. For example, for zero velocities at the boundaries, the unconstrained minimum acceleration model predicts

$$T = \sqrt{\frac{6L}{\left|\ddot{\boldsymbol{r}}(0)\right|}} \tag{20}$$

which manifests a square root law relating the movement extent to its total duration. Therefore, if rapid arm movements are well predicted using the minimum acceleration model, then the duration of the movement is locally encoded in the initial (final) acceleration of the hand. Equations (18) and (20) provide different predictions for point-to-point movement duration, which can be studied empirically (see [40]).

For via-point and path-constrained movements, however, predicting the total duration from the local kinematics is more delicate. To approach this problem, we use the constant of motion of path-constrained minimum jerk trajectories, D_3, (16)

$$\boldsymbol{r}^{(1)} \cdot \boldsymbol{r}^{(5)} - 2\boldsymbol{r}^{(2)} \cdot \boldsymbol{r}^{(4)} + \boldsymbol{r}^{(3)} \cdot \boldsymbol{r}^{(3)} = D_3.$$

For a known set of boundary conditions, the duration of the movement, T, can be computed locally from the time invariant constant D_3. The total duration is defined by taking a definite integral

$$D_3 \cdot T = 5A_3(T) + 2\dot{\boldsymbol{r}} \cdot \boldsymbol{r}^{(4)} - 4\ddot{\boldsymbol{r}} \cdot \dddot{\boldsymbol{r}} \Big|_0^T \tag{21}$$

where the $\cdot$ notation is used for inner products in $\mathbb{E}^d$, and $A_3(T)$ is the total squared norm of jerk accumulated in the time interval $[0, T]$. This is a characteristic equation for movement duration in the unconstrained and constrained minimum jerk optimization schemes.

For via-point optimization, we showed in the previous section [see (17)–(44)] that the constants D_3^i defined between via-points and or endpoints are equal to each other. It is now possible to sum all terms $D_3^i \cdot T_i$ defined between via-points, where T_i is the duration between the $(i-1)$th and the ith via-points

$$\begin{aligned} D_3 \cdot T &= \sum_i D_3^i \cdot T_i \\ &= \sum_i 5A_3(t_{i-1}, t_i) + 2\dot{\boldsymbol{r}} \cdot \boldsymbol{r}^{(4)} - 4\ddot{\boldsymbol{r}} \cdot \dddot{\boldsymbol{r}} \Big|_{t_{i-1}}^{t_i} \\ &= 5A_3 + 2\dot{\boldsymbol{r}} \cdot \boldsymbol{r}^{(4)} - 4\ddot{\boldsymbol{r}} \cdot \dddot{\boldsymbol{r}} \Big|_0^T. \end{aligned} \tag{22}$$

Hence, the total duration can also be predicted from the combination of local (the constant of motion D_3) and global properties (the total cost A_3) in the case of multiple via-point optimization. This analysis reveals a local-global regularity for the minimum jerk optimization of all of the motor tasks considered here: unconstrained, via-point, and path-constrained movements

$$T = \frac{1}{D_3}\left(5A_3 + 2\dot{\boldsymbol{r}} \cdot \boldsymbol{r}^{(4)} - 4\ddot{\boldsymbol{r}} \cdot \dddot{\boldsymbol{r}} \Big|_0^T\right). \tag{23}$$

Similarly, for the unconstrained, via-point, and path-constrained minimum acceleration optimization schemes

$$T = \frac{1}{D_2}\left(-\frac{3}{2}A_2 + \dot{\boldsymbol{r}} \cdot \ddot{\boldsymbol{r}} \Big|_0^T\right). \tag{24}$$

The above derivations hold for general dimension d and can be readily generalized to the MSD model of order n.

Fitts' law: The predictions from the last section can now be used to succinctly represent the square root variant of Fitts' law [33] (for alternative formulation, see [41]). According to this variant of Fitts' law [40], [42], movement duration is dictated by

$$T = \sqrt{\frac{L}{W}} \tag{25}$$

where W is the width of the target of the movement in task space or, alternatively, the tolerated task-space error of the end-effector at the target at the end of the movement.

Direct algebraic manipulations show that the following rules are equivalent to the Fitts' law variant (25). For unconstrained minimum jerk movements with zero velocities and accelerations at the endpoints

$$T = \frac{7}{5!}\frac{A_2}{W^2}, \quad \frac{A_3}{A_2} = \frac{7!}{5!}\frac{W}{L} \tag{26}$$

where A_2 and A_3 are the L^2 norms of the acceleration and jerk profiles, respectively. The second equation is of particular interest, since it predicts Fitts' law without a direct constraint on the duration of movement. For unconstrained minimum acceleration movements with zero velocities at the boundaries

$$\ddot{\boldsymbol{r}}(0) = 6W, \quad \text{Initial acceleration-Fitts}' \text{ law}.$$

According to the last prediction, the acceleration at the endpoints is proportional to the target's width; for a very small target, the speed near the target slowly decreases to zero, consistent with the requirement of higher accuracy in this case. This shows that Fitts' law can be predicted by assuming a regularity in local parameters (e.g., initial jerk) or global parameters (e.g., total cost) [see also [40] and Table 1].

TABLE 1
FITTS' LAW EQUIVALENT RULES

Equation	Rule
$T = \sqrt{\frac{L}{W}}$	SQR Fitts' law variant [42]
$A_3 = 6!\sqrt{\frac{W^5}{L}}$	Total jerk
$\frac{A_2}{T} = \frac{5!}{7}W^2$	Mean acceleration
$D = 6!\frac{5W^3}{L}$	Ratio of total jerk and acceleration

III. PRIMITIVE GUIDED SMOOTH MOVEMENT GENERATION

We now formulate the model and derive the computational tools underlying the main contribution of this paper—optimal, swift, and invariant adaptation of movement production to a desired task-space plan. We start by introducing the equation defining how movements are adapted from a template trajectory, while fulfilling new boundary conditions (movement regeneration).

The jerk–accuracy equation: A task-space trajectory $\boldsymbol{r}(t)$ is generated based on a desired template trajectory in task space

$$\boldsymbol{r_0}(t).$$

The smoothness of $\boldsymbol{r}(t)$ is maximized under the constraint that $\boldsymbol{r}(t)$ follows the template trajectory $\boldsymbol{r_0}(t)$. This smoothness maximization is achieved by minimizing a cost function

$$\min_{\boldsymbol{r}} I\left(\boldsymbol{r_0}, \boldsymbol{r}, \frac{d}{dt}\boldsymbol{r}, \ldots, \frac{d^n}{dt^n}\boldsymbol{r}\right) \tag{27}$$

for a performance index I of the form

$$I = \text{OC}\left(\frac{d}{dt}\boldsymbol{r}, \ldots, \frac{d^n}{dt^n}\boldsymbol{r}\right) + \lambda \cdot \text{ERC}\left(\boldsymbol{r_0}, \boldsymbol{r}\right)$$

that represents a tradeoff between OC (optimality criterion) and ERC (error criterion) [12].

Variational calculus shows that for any $\lambda \in \mathbb{R}$, solutions to (27) are minimizations of OC subject to a specific error ERC(λ),

and conversely, solutions to (27) are minimizations of ERC subject to a specific optimal cost OC(λ), where λ is a Lagrange multiplier. Hence, the derived optimal trajectories are the most accurate or the most smooth possible trajectories, for a required optimality cost or accuracy constraint, respectively.

Previous studies have investigated several models of jerk minimization, which included mainly jerk minimization subject to predefined task constraints—boundary conditions, via-points, and the exact path of the movement. We now formulate a new model that predicts the trajectory of a movement based on a template trajectory or a template path. First, we solve the general case of an arbitrary template trajectory and then we introduce a special solution derived by assuming the optimality of the template (see Section II-B). For now, this template need not be optimal and is defined as

$$\boldsymbol{r_0}(t) \in \text{task space} \quad \forall t \in [0, T]$$

where T is the duration of the movement for the entire template. The JA functional has the form of (27)

$$I_{\boldsymbol{r_0},T,\lambda}(\boldsymbol{r}, \dddot{\boldsymbol{r}}) = \int_0^T |\dddot{\boldsymbol{r}}|^2 dt + \lambda^6 \int_0^T |\boldsymbol{r} - \boldsymbol{r_0}|^2 dt \quad (28)$$

which implements a tradeoff between the minimization of jerk (OC) and the maximization of accuracy (ERC), where the constant λ^6 (Lagrange multiplier) modulates the weighting of the two costs. The second term in (28) represents the L^2 norm of the time-dependent distance between $\boldsymbol{r_0}$ and $\boldsymbol{r}$. As in the case of the previous minimum jerk formulations, the above minimization is subject to an arbitrary choice of boundary conditions $\boldsymbol{B}$, which fix the endpoint positions, velocities, and accelerations.

The EL equations can then be derived and solved

$$\sum_k (-1)^k \frac{d^k}{dt^k} \frac{\partial L}{\partial \boldsymbol{r}^{(k)}} = 0$$

$$L(\boldsymbol{r}, \dot{\boldsymbol{r}}, \ddot{\boldsymbol{r}}, \dddot{\boldsymbol{r}}, t) = |\dddot{\boldsymbol{r}}(t)|^2 + \lambda^6 |\boldsymbol{r}(t) - \boldsymbol{r_0}(t)|^2. \quad (29)$$

The solution satisfies the equation

$$\boldsymbol{r}^{(6)}(t) = \lambda^6 \left(\boldsymbol{r}(t) - \boldsymbol{r_0}(t)\right) \quad (30)$$

where the right-hand side, $\lambda^6 \left(\boldsymbol{r}(t) - \boldsymbol{r_0}(t)\right)$, is the weighted vector measuring the error between the optimal solution and the prescribed template curve. This gives a tradeoff between jerk and accuracy for the optimal solution, solved by the trajectory whose sixth-order time derivatives point in the direction of the time-dependent error vector, i.e., from the optimal trajectory to the template curve, and is proportional to the error.

A. Reaching Movements

We now explore the predictions of the JA model (30) for reaching movements by assuming smoothness maximization and the global accuracy of the movement with respect to the movement's target. The equations derived below show that for reaching movements, the JA optimization has a closed-form solution. Depending on the accuracy demands at the target point, this optimization predicts movement reversals around the target, caused by higher accuracy demands.

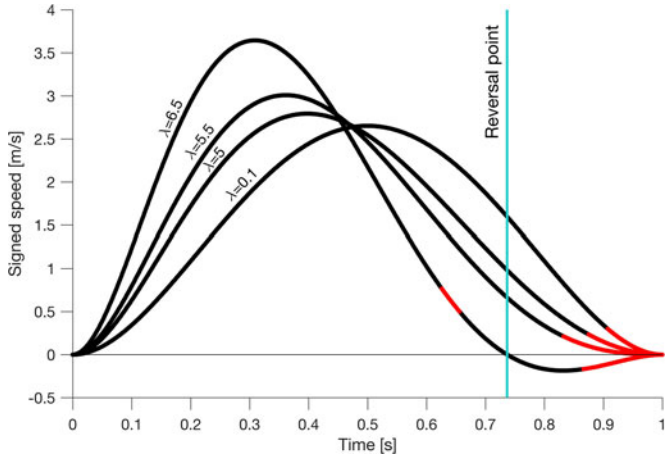

Fig. 2. Speed profiles of endpoint accuracy trajectories. The trajectories whose speed profiles are depicted were constructed by defining a JA cost, using different accuracy demands at the endpoint, by minimizing $\int_0^1 x^{\cdots 2} dt + \lambda \int_0^1 (x - x_{\text{end}})^2 dt$ for different lambdas. The red color marks the part of the trajectory $x(t)$ near the target, $|x(t) - x_{\text{end}}| \leq 0.01 \cdot |x_{\text{end}} - x_{\text{start}}|$. For the largest accuracy demand ($\lambda = 6.5$), the model predicts movement reversal between $t = 0.7$ and $t = 0.8$ (turquoise line). For this trajectory, the acceleration at the reversal point is not zero, as predicted by a point-to-point minimum jerk trajectory for simple reaching movements.

Although the speed profiles of the hand are bell shaped in reaching movement [3], these profiles are affected by demands for movement accuracy and the total duration required by the motor task [6]. For rapid arm movements requiring accuracy at the target, the speed profiles show a long tail as the hand approaches the target. In extreme cases, rapid arm movements may include movement reversals whereby the hand overshoots the target and then produces a "corrective movement" in the opposite direction. This behavior can be modeled using the JA functional (28) by assuming that the goal of the movement is to minimize the time-dependent error from the target. Hence, the template of the movement is the target

$$\boldsymbol{r_0}(t) \equiv \boldsymbol{r}_{\text{target}}.$$

Then, according to (30)

$$\boldsymbol{r}^{(6)}(t) = \lambda^6 \left(\boldsymbol{r}(t) - \boldsymbol{r}_{\text{target}}\right).$$

The general solution for 2-D task space has the form

$$\boldsymbol{r}(t) = \boldsymbol{r}_{\text{target}} + \boldsymbol{A} \begin{pmatrix} e^{\lambda t} \\ e^{-\lambda t} \end{pmatrix} + \boldsymbol{B} \begin{pmatrix} \sin\theta t \\ \cos\theta t \end{pmatrix} e^{-\frac{\lambda}{2} t} + \boldsymbol{C} \begin{pmatrix} \sin\theta t \\ \cos\theta t \end{pmatrix} e^{\frac{\lambda}{2} t} \quad (31)$$

where $\theta = \frac{\lambda\sqrt{3}}{2}$, and the coefficients of the matrices $\boldsymbol{A}, \boldsymbol{B}, \boldsymbol{C} \in \mathbb{R}^{2\times 2}$ are linear functions of the boundary conditions $\boldsymbol{r}(0), \boldsymbol{r}(T), \dot{\boldsymbol{r}}(0), \dot{\boldsymbol{r}}(T), \ddot{\boldsymbol{r}}(0)$, and $\ddot{\boldsymbol{r}}(T)$. Fig. 2 plots the speed profiles for a straight movement with zero speeds and accelerations at the endpoints. Our model predicts movement reversals using a global optimization instead of appending a corrective movement to an ongoing movement. For a larger coefficient λ, the speed profile becomes left-skewed to increase the

accuracy, here measured by spatial error, at the target. There is a critical accuracy level (a critical value $\lambda = \lambda_c$), for which the optimal movement overshoots the target and then reverses in order to minimize the error near the target. This phenomenon is also observed in rapid human reaching movements with high accuracy demands [43]. In general, (31) predicts the reaching movement trajectory based on arbitrary boundary conditions, and therefore the predicted movement is not limited to the case of zero velocities and accelerations at the endpoints and is not necessarily straight.

B. Movement Generation Based on a Polynomial Template

Above, we used the JA formulation to predict reaching movements by regenerating a simple template trajectory defined by a fixed-point trajectory located at the movement's target. Here, we generalize this to the case of a template trajectory in the form of a trajectory whose task-space coordinates are general time-dependent polynomials. As in the case of reaching movements, we present the solution in a closed form.

We assume that the template is given by a time polynomial trajectory, $\boldsymbol{r_0}(t) = \sum_{i=0}^{N} \boldsymbol{a_i} t^i$, where $\boldsymbol{a_i} \in \mathbb{R}^2$. We solve for the smoothest update of the polynomial trajectory that complies with newly introduced endpoint positions, velocities, and accelerations, and a tolerated total error $\int_0^T |\boldsymbol{r}(t) - \boldsymbol{r_0}(t)|^2 \, dt$. For brevity, we introduce the solution for a template satisfying (3) (i.e., $N = 5$), i.e., minimizing jerk for a point-to-point boundary conditions.

The optimal trajectory (MG based on the polynomial template) must satisfy [see (28)]

$$\boldsymbol{r}^{(6)}_{\text{opt}}(t) = \lambda^6 \left(\boldsymbol{r}_{\text{opt}}(t) - \sum_{i=0}^{N} \boldsymbol{a_i} t^i \right). \tag{32}$$

The solution of (32) is given by assuming the following superposition:

$$\boldsymbol{r}_{\text{opt}}(t) = \boldsymbol{p}(t) + \sum_{i=1}^{6} \boldsymbol{k_i} \exp(\theta_i t)$$

where the 2-D polynomial $\boldsymbol{p}(t)$ and the arguments θ_i are solved by substituting $\boldsymbol{r}_{\text{opt}}(t)$ in (32) above

$$\theta_i = \sqrt[6]{1}\lambda, \qquad \boldsymbol{p}(t) = \sum_{i=0}^{N} \boldsymbol{a_i} t^i \tag{33}$$

and the vectors $\boldsymbol{k_i} \in \mathbb{R}^2$ are found by satisfying the boundary conditions. Using the Euler identity, we can express the generally complex exponential relations using real-valued logarithmic spirals. The optimal solution is a superposition of the polynomial template and affine transformations of a hyperbola and two logarithmic spirals:

$$\begin{aligned} \boldsymbol{r}_{\text{opt}}(t) = & \sum_{i=0}^{N} \boldsymbol{a_i} t^i + \boldsymbol{A} \begin{pmatrix} e^{\lambda t} \\ e^{-\lambda t} \end{pmatrix} \\ & + \boldsymbol{B} \begin{pmatrix} \sin\theta t \\ \cos\theta t \end{pmatrix} e^{-\frac{\lambda}{2} t} + \boldsymbol{C} \begin{pmatrix} \sin\theta t \\ \cos\theta t \end{pmatrix} e^{\frac{\lambda}{2} t} \end{aligned} \tag{34}$$

where $\theta = \frac{\lambda\sqrt{3}}{2}$, and the matrices $\boldsymbol{A}, \boldsymbol{B}, \boldsymbol{C} \in \mathbb{R}^{2\times 2}$ are composed of the above $\boldsymbol{k}_i$ as column vectors.

Using affine orbits: Up to translation, an affine orbit $\boldsymbol{O_A}(t)$ has the form

$$\boldsymbol{O_A}(t) = \exp(\boldsymbol{A}t)\boldsymbol{p}_0 \tag{35}$$

where $\boldsymbol{A} \in \mathbb{R}^{2\times 2}$ is any matrix, and $\boldsymbol{p_0} \in \mathbb{R}^2$ is any vector. We now show that the optimal trajectory $\boldsymbol{r}(t)$ is a superposition of affine orbits with the template $\boldsymbol{p}(t)$.

Equation (32) can also be solved using a matrix form. We assume a private solution $\boldsymbol{r_A}(t)$ of the form

$$\boldsymbol{r_A}(t) = \boldsymbol{p}(t) + \exp(\lambda \boldsymbol{A}t)\boldsymbol{p_0} \tag{36}$$

where $\boldsymbol{A} \in \mathbb{R}^{2\times 2}$, $\boldsymbol{p_0} \neq \boldsymbol{0} \in \mathbb{R}^2$, and $\boldsymbol{p}(t)$ is a 2-D fifth-order time polynomial. Let us substitute (36) in (32) and solve for $\boldsymbol{A}$

$$\begin{aligned} \boldsymbol{r}^{(6)}_{\boldsymbol{A}}(t) = & \ (\lambda \boldsymbol{A})^6 \left(\boldsymbol{r_A}(t) - \boldsymbol{p}(t) \right) \\ = & \ \lambda^6 \left(\boldsymbol{r_A}(t) - \sum_{i=0}^{N} \boldsymbol{a}_i t^i \right). \end{aligned}$$

If $\lambda \neq 0$, we find that $\boldsymbol{A}$ and the polynomial $\boldsymbol{p}(t)$ satisfy

$$\boldsymbol{p}(t) = \sum_{i=0}^{N} \boldsymbol{a_i} t^i, \qquad \boldsymbol{A}^6 = \boldsymbol{I} \tag{37}$$

where $\boldsymbol{I}$ is the identity matrix. We solve for a real-valued matrix $\boldsymbol{A}$. Turnbull [44] solved the matrix equation $\boldsymbol{\xi}^3 = \boldsymbol{I}$ using integer entries. The square root of $\boldsymbol{\xi}$ can also be given by integer entries. We obtain

$$\boldsymbol{\xi} = \begin{pmatrix} -1 & 1 \\ -1 & 0 \end{pmatrix}, \qquad \boldsymbol{\zeta} = \begin{pmatrix} 0 & 1 \\ -1 & 1 \end{pmatrix}.$$

The matrix $\boldsymbol{\zeta}$ thus generates a sixth-order cyclic group, and solutions to the second part of (37) are

$$\boldsymbol{A_k} = \boldsymbol{\zeta}^k, \text{ for any } k. \tag{38}$$

The order of (30) is six; therefore, the general solution to (32) is

$$\begin{aligned} \boldsymbol{r}(t) = & \ \boldsymbol{p}(t) + \sum_{k=1}^{6} \exp(\lambda \boldsymbol{A_i} t)\boldsymbol{p_i} \\ = & \ \boldsymbol{p}(t) + \exp(\lambda \boldsymbol{A_1} t)\boldsymbol{p_1} + \exp(\lambda \boldsymbol{A_1}^2 t)\boldsymbol{p_2} + \exp(-\lambda \boldsymbol{I} t)\boldsymbol{p_3} \\ & + \exp(-\lambda \boldsymbol{A_1} t)\boldsymbol{p_4} + \exp(-\lambda \boldsymbol{A_1}^2 t)\boldsymbol{p_5} + \exp(\lambda \boldsymbol{I} t)\boldsymbol{p_6} \end{aligned} \tag{39}$$

where the points $\boldsymbol{p_1}, \ldots, \boldsymbol{p_6} \in \mathbb{R}^2$ are determined by satisfying boundary conditions by solving a linear system of equations in the endpoint positions, velocities, and accelerations. The summands in (39) are called affine orbits in the affine geometry of planar curves [45], and the matrices

$$\boldsymbol{A_k} = \begin{pmatrix} 0 & 1 \\ -1 & 1 \end{pmatrix}^k$$

are examples of (Lie algebra) generators of such affine orbits. Extending this MG equation to 3-D task space requires identifying a matrix subgroup of order six as in (38).

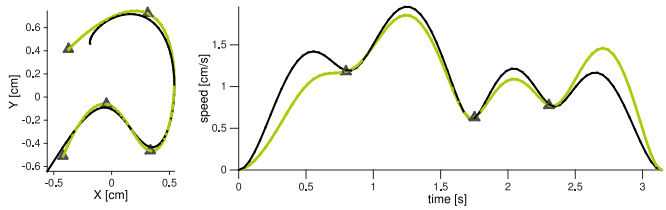

Fig. 3. JA regeneration of a template (numerical trajectory). The template (green) was defined using a set of via-points (triangles) (9) [3]. The JA trajectory (black) was numerically computed based on the template by spatially perturbing the endpoint positions of the template (see Section III-C). (Left) Task-space paths. (Right) Speed profiles.

A generalization of the notion of Euclidean curvature in Euclidean geometry to the affine geometry, called (full-) affine curvature [2], is constant along each affine orbit [45]. Moreover, the affine curvatures of the summands in (39) are independent of the vectors $\boldsymbol{p_i}$ [45]; hence, the affine orbits can serve as geometrical building blocks.

C. Numerical Algorithm for Maximally Smooth Regeneration

The sections above introduced the JA cost function and the necessary conditions for maximizing smoothness with respect to a template trajectory. We used this model to predict the trajectory of rapid reaching movements by assuming that the template trajectory is a fixed point in task space, defined by the target of the reaching movement. This formulation was generalized to the case in which the template trajectory is a fifth-order time polynomial (any high-dimensional task-space trajectory represented by coordinates with time polynomial dependence can be used). We now present the general case of smoothness maximization with respect to an arbitrary template trajectory.

The optimal trajectory regeneration defined by (30) can be formulated as a boundary value problem (BVP) and then computed using a three-stage Lobatto IIIa formula (MATLAB function, bvp4c [46]). This algorithm efficiently solves for the minimal jerk trajectory, which accurately follows a template trajectory. The template trajectory is represented by an ordered set of points in task space ("point-cloud").

Fig. 3 depicts the result of JA regeneration of a numerical trajectory (template). The numerical template in this example was defined as the minimal jerk trajectory passing through a prescribed set of task-space via-points (derived through (9) [3] and algorithm in [4]). The via-points were selected to form a minimal jerk trajectory, whose shape followed the Hebrew letter Bet. The trajectory was sampled and then processed as a numerical template for regeneration, as defined above. The template is drawn in green and the optimal JA trajectory, derived as explained above, in black, and triangles mark the via-points on the template trajectory. The JA trajectory was generated from the numerical template using a tradeoff value of $\lambda = 8$ (30) and by introducing new start and end locations that deviated from the original template's endpoints. In spatial terms (Fig. 3, left panel), the largest errors between the template and the updated smoothest trajectory appeared near the via-points, approximately near the maxima of curvature of the template. However, in terms of velocity (right panel), the errors in the vicinity of the via-points were the smallest.

Fig. 4 depicts the trajectories resulting from numerically solving the JA equation solving BVP for different accuracy thresholds λ. The value of λ determines an optimal tradeoff between generating point-to-point movement as in (3) and closely generating the original trajectory, while in all cases satisfying the new required boundary conditions. Hence, the actual trajectory has different boundary conditions than those of the desired trajectory. Generating highly accurate trajectories (large λ) causes undesired increase in the high-order time derivatives at the endpoints [see Fig. 4(h)].

Regeneration of noisy trajectories: We now test the performance of the numerical MG algorithm in the case of a noisy template trajectory. The noisy template is generated by sampling and adding Gaussian noise to an analytic trajectory whose high-order time derivatives are known. We then regenerate a smooth trajectory from the noisy sampled trajectory and compare the time derivatives of the smooth trajectory to those of the analytic one that serves as a ground truth (GT).

Fig. 5 compares the estimation of high-order time derivatives using low-pass filtered trajectories with those smoothed using the JA model. First, a GT trajectory whose derivatives are known was computed and sampled $(N = 200)$ based on (9). Then, to simulate a noisy trajectory, the GT trajectory was contaminated with Gaussian noise. Finally, the noisy trajectory was smoothed using a finite impulse response (FIR) low-pass filter (length $N = 25$) and the JA model $(\lambda = 25)$. The cutoff frequency of the filter corresponded to 2 Hz for a 2-s trajectory. The top panel in Fig. 5 shows the GT and noisy trajectories. The bottom panels show the magnitude of the first- to fifth-order time derivatives (magnitudes of velocity, acceleration, jerk, snap, and crackle). The trajectories and the magnitude of time derivatives of the GT (black), noisy (blue), low-pass filtered (pink), and JA (green) were plotted on the same axis for comparison. The JA outperformed the FIR filtering approach with respect to the derivation of higher order time derivatives.

IV. Variance and Invariance of Mean-Squared Derivative Optimization

As for many variational problems in physics, we can distinguish between off-shell invariance versus on-shell invariance under a given group of transformations of the unknown function, including its boundary conditions: In the first case, the Lagrangian or the EL equations are themselves invariant under the transformations, whereas in the second case, the transformation applied to any solution gives another solution.

In what follows, we examine several jerk-minimization problems, which are invariant under affine transformations in the sense of on shell invariance. We point out that any point-to-point MSD optimization scheme, as in (1), as well as the JA minimization presented in this paper (28) are affine-invariant using this notion of invariance. We also show that the via-point and path-constrained MSD optimization problems are not affine invariant according to this definition.

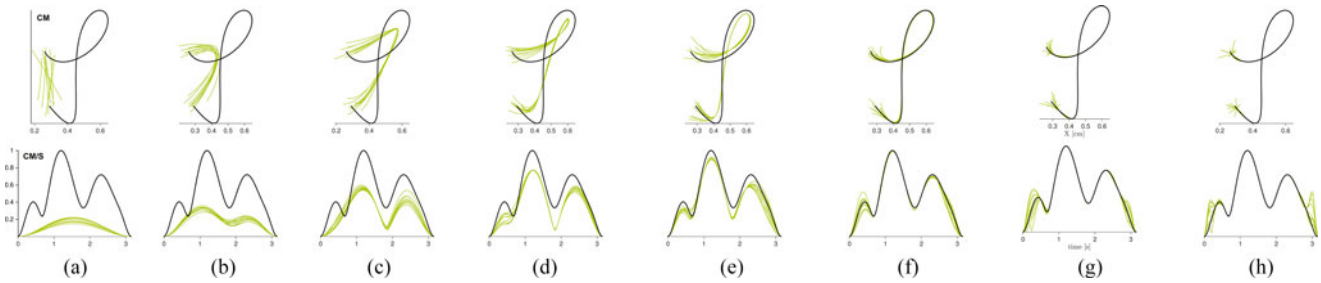

Fig. 4. Optimal JA trajectories (green) calculated using different accuracy thresholds λ for a template modeling a human drawing movement. The template (black) was generated using the via-point minimum jerk model using four via-points. Trials were formed by perturbing the initial and final positions of the template for each value of λ and then calculating the JA update (see Section III-C). The larger the λ, the more accurate the generated trajectories. For $\lambda = 1$, the paths and the speed profiles were close to the optimal unconstrained minimum jerk for point-to-point movements, and for $\lambda = 15$, the generated trajectories closely reproduced the template such that the perturbed boundary conditions were satisfied. (Top) Task space. (Bottom) Speed profiles.

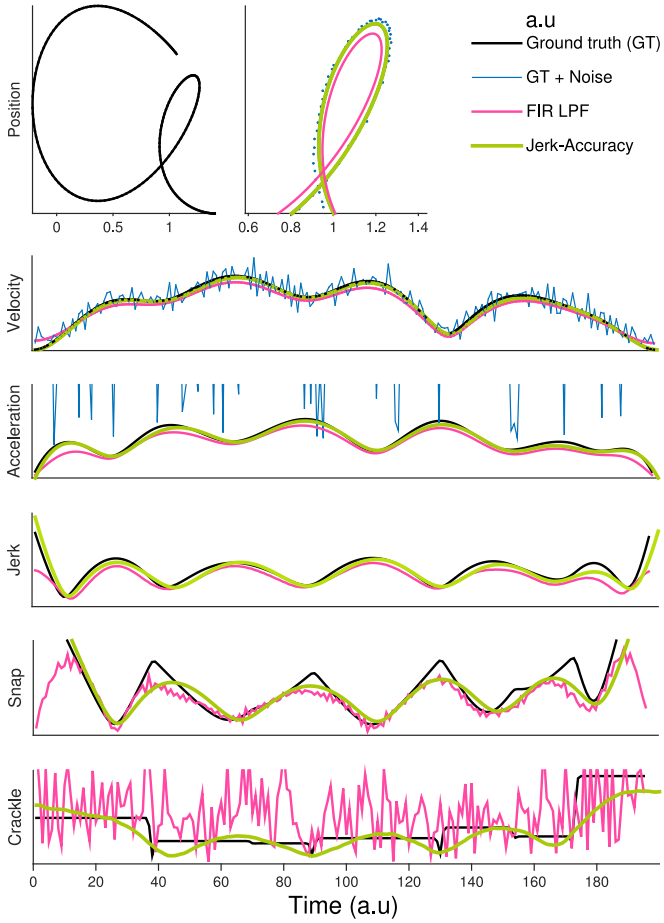

Fig. 5. Accuracy of high-order time derivatives. Noise was added to an analytically generated GT trajectory (top left and right panels), whose derivatives were determined numerically. The bottom panels show the magnitude of the first to fifth-order time derivatives (velocity, acceleration, jerk, snap, and crackle) for the GT (black), noisy (blue) FIR low-pass filtered (LPF) (pink) and JA (green) trajectories. The JA model unraveled the correct trend of the true high-order derivatives (see Section III-C).

For two different sets of task-dependent constraints (e.g., boundary conditions) associated with each other through an affine transformation, the solution satisfying the second set of constraints is the affine transformation of the optimal solution satisfying the first set of constraints. We call this an invariance to the transformation of the motor task. The effect of such transformations on movement optimization has not been studied before in the context of human movement (but see [47]).

The derivations in this section apply to a general task-space dimension d.

A. Affine Invariance of Point-to-Point Mean-Squared Derivative Optimization

Consider a motor-task described by a desired template $\boldsymbol{r_0}(t)$, required boundary conditions $\boldsymbol{B}$, and the optimal regeneration $\boldsymbol{r}(t)$. Then, an affine transformation $\boldsymbol{M}$ of $\boldsymbol{r}$ and $\boldsymbol{B}$ defines a new motor task such that $\boldsymbol{q} = \boldsymbol{M}(\boldsymbol{r})$ and $\boldsymbol{C} = \boldsymbol{M}(\boldsymbol{B})$. The optimal regeneration of $\boldsymbol{q}$ satisfying the new boundary conditions $\boldsymbol{C}$ is the affine transformation of the original motor task:

$$\boldsymbol{q}(t) = \boldsymbol{M}(\boldsymbol{r}(t)) \quad \forall t. \tag{40}$$

This stems from the linearity of the set of differential operators defining the boundary conditions, which fully impose a unique solution, and the fact that the complete solution space is closed under affine transformations. Thus, planning a maximally smooth movement based on requirements at the boundaries can be done *a priori*, while movement production is achieved by an affine transformation of the trajectory plan and the template, which is useful not only for fast motion replanning in the presence of perturbations but also for motion generalization in learning from demonstration.

B. Affine Invariance of Jerk–Accuracy Minimization

It appears that the notion above of affine invariance holds also for the JA minimization, as in (28). This seems unexpected at first, since the distance $\boldsymbol{r} - \boldsymbol{r_0}$ in the second term of (28) is not invariant to a joint linear transformations of $\boldsymbol{r}$ and $\boldsymbol{r_0}$.

Let us consider a template $\boldsymbol{r}_0(t)$ and a new template $\boldsymbol{r}_{\text{new}}(t)$ that is defined from an affine transformation $\boldsymbol{M}$ of $\boldsymbol{r}_0(t)$: $\boldsymbol{r}_{\text{new}}(t) = \boldsymbol{M}(\boldsymbol{r}_0(t))$. The affine invariance can be readily deduced from (30). Let us assume that $\boldsymbol{r(t)}$ is an optimal MG of a template $\boldsymbol{r_0}$ with accuracy demand λ and boundary conditions $\boldsymbol{B}$ according to (30); then, the transformed trajectory $\boldsymbol{M}(\boldsymbol{r})$ satisfies

$$\frac{d^6}{dt^6}\boldsymbol{M}(\boldsymbol{r}(t)) = \lambda^6 \left(\boldsymbol{M}(\boldsymbol{r}(t)) - \boldsymbol{r}_{\text{new}}(t)\right) \tag{41}$$

with boundary conditions $\boldsymbol{M}(\boldsymbol{B})$. This invariance stems from (30), which states that the direction of the error vector between the template and the optimal trajectory has to point in the direction of the sixth-order time derivative of the optimal trajectory, while both the colinearity and the differentiation are affine invariant.

C. Euclidean but Not Affine Invariance of Constrained Tasks

For path-constrained jerk minimization [4], we proved that any optimal solution must satisfy a Euclidean constraint, namely, that the sixth-order time derivative is perpendicular to the tangent to the curve (12). Therefore, affine transformations of tasks and optimal movements in such constrained cases lead to trajectories that are not optimally smooth.

Similarly (9) and (10) are not affine invariant due to the Euclidean requirement at the via-point. A precise selection of duration from the beginning of the movement to the via-point results in a vector difference between the fifth-order derivatives before and after the via-point, which is perpendicular to the tangent to the trajectory at the via-point. This implies that the optimal time at the via-point changes following affine transformations. Hence, one cannot obtain trajectories that satisfy the boundary conditions, go through the via-point, and remain optimal following an affine transformation.

We conclude that the via-point and the path-constrained tasks are invariant only under Euclidean transformations, whereas the unconstrained minimum jerk is invariant under the more general affine transformations.

V. Real-Time Movement Generation: Simulation and Evaluation

The theoretical and computational approaches used to derive the JA model were described above. In this section, we use the JA formulation to design a real-time MG algorithm that is capable of producing smooth and accurate trajectories in the presence of perturbations applied to the end-effector or the movement's target. Achieving real-time performance is possible due to the linearity of the vectors $\boldsymbol{p_i}$ (39) in the required boundary conditions, which are defined to satisfy the kinematics resulting from the applied perturbation.

We demonstrate the accuracy and smoothness of the JA real-time MG algorithm and compare its performance to that of other MG algorithms used in robotics, focusing on (1) the competence (accuracy) and (2) the smoothness of the regenerated trajectories. Four algorithms dealing with MG in the presence of noise and perturbations are compared to our approach. The evaluation is based on a recent benchmark system [28] developed to assess the human likeness and performance of trajectory planning algorithms for robotic systems.

A. Real-Time Optimal Regeneration of Arbitrarily Complex Trajectories

We now develop a real-time approach that employs (28) to regenerate a human trajectory, which is providing a demonstration for a robotic system (human demonstration). This human-inspired MG is later compared to trajectories of human movements. We call this method real-time jerk-accuracy movement regeneration algorithm (RTJAMG).

We separate the regeneration problem into an offline learning stage (planning the template) and an online MG stage (adaptive generation). The template is given here by a human demonstration, consisting of a trajectory of the form $\boldsymbol{r_0}(t) : [0, T] \rightarrow \mathbb{R}^2$, where T is the duration of the demonstration. Our algorithm continuously plans a portion of movement that is an optimal update of the learned/represented trajectory using boundary conditions that can be externally perturbed/updated. The use of affine deformations in adaptive motion planning in robotics was first suggested in [47].

The approach described below uses the linearity in the boundary conditions in (39). This allows executing the optimal movement plan based on an efficient linear computation and thus real-time recovery from various perturbations.

1) Planning and Learning: For simplicity, we present a naive approach, which uses the human demonstration as a movement plan to be regenerated. The method presented below does not attempt to use the human demonstration to infer a movement policy as in other recent approaches [48]–[51].

Input: $\boldsymbol{r_0}(t)$
Output: $\boldsymbol{r_1}(t), \lambda, W_0$
1: $\boldsymbol{r_1}(t) \leftarrow$ OptimalFilter($\boldsymbol{r_0}(t)$) {we use the JA approach for scatter data, Section III-C}
2: $W_0 \leftarrow$ OptimizeWindow($\boldsymbol{r_1}(t)$) {We leave this as a constant}
3: $\lambda \leftarrow$ Complexity($\boldsymbol{r_1}(t)$) {We leave this as a constant}

2) Movement Generation: The MG algorithm uses the closed-form regeneration of trajectories with polynomial time dependence (39). Stable production under possibly continuous unknown perturbations is solved in a closed loop in which the information about the perturbation is processed to allow recovery of the robotic or human end-effector. The following algorithm accepts the current state of the plant and the time and informs the next velocity command. We assume a preprocessed template $\boldsymbol{r_1}(t)$, a time window W_0, and a JA parameter λ.

Input: $\boldsymbol{x}(t), \boldsymbol{v}(t), t$ {position, velocity and time}
Output: $\boldsymbol{v}_{\text{next}}$
1: $\boldsymbol{B_1} \leftarrow [\boldsymbol{x}, \boldsymbol{v}, \boldsymbol{0}]$ {Initial Condition}
2: $\boldsymbol{B_2} \leftarrow [\boldsymbol{r_1}(t + W_0), \dot{\boldsymbol{r}}_{\boldsymbol{1}}(t + W_0), \boldsymbol{0}]$ {Endpoint Condition}
3: $\boldsymbol{p}(t) \leftarrow$ GetPolynomial($\boldsymbol{B_1}, \boldsymbol{B_2}$) {(3)}
4: $\{\boldsymbol{p_1}, \ldots, \boldsymbol{p_6}\} \leftarrow$ OrbitCoefficients($\boldsymbol{p}, \boldsymbol{B_1}, \boldsymbol{B_2}$)
5: $\boldsymbol{r}(t) \leftarrow$ OrbitEquation($\boldsymbol{p}, \boldsymbol{p_1}, \ldots, \boldsymbol{p_6}$)
6: $\boldsymbol{v}_{\text{next}} \leftarrow \dot{\boldsymbol{r}}(t)$

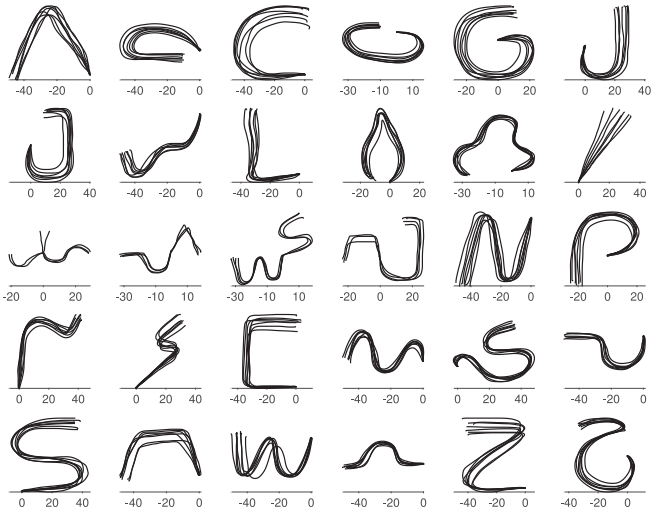

Fig. 6. Task-space human demonstrations used in the benchmark evaluation. The dataset (LASA lab, EPFL, part of the EU AMARSi project) consists of 30 shapes drawn repeatedly $(N = 7)$ by one subject whose movements were captured using a computer tablet.

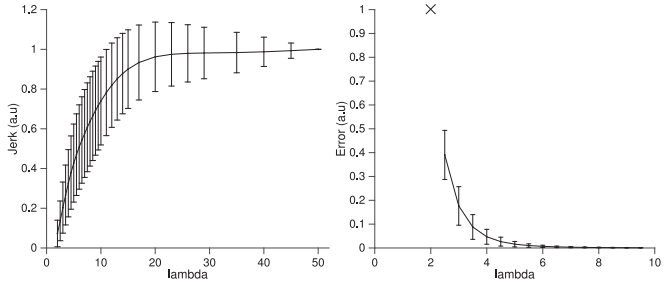

Fig. 7. Tradeoff between smoothness and accuracy in regeneration of human trajectories using the JA model. Human trajectories (see Fig. 6) were regenerated repeatedly based on (28), solving a BVP using the endpoint kinematics of the human trajectories. Averages were calculated across repetitions (7) and shapes (30) and error bars across shapes. For large λ (a strong accuracy requirement), the total jerk in the reproductions reached that of the human demonstrations (left panel) and the error dropped to zero (right panel), whereas for small λ, the total jerk in the reproductions reached that of the unconstrained minimum jerk model [3], and the error was largest.

B. Alternative Approaches in the Benchmark Evaluation

The performance of three algorithms were compared with the JA algorithm.

1) A task-parameterized Gaussian mixture model (TpGMM) [49], which implements a virtual spring damper system.
2) A probabilistic approach for movement primitives called probabilistic movement primitives [51]. The motion is represented as a distribution over trajectories used as a stochastic feedback controller that can reproduce similar trajectories given the corresponding distribution.
3) Control Lyapunov function-based dynamic movements (CLF-DM)[50]. This approach builds an estimate of an energy function generalized from user demonstrations used during runtime to ensure global asymptotic stability of nonlinear dynamical systems at the target.

All models were implemented and provided by their authors (see [28]).

C. Benchmark System

We compared the performance of the RTJAMG (see Section V-I) with that of other recently published algorithms dealing with similar problems in regenerating human drawing movements (see Section V-B). Performance was compared in four motor scenarios based on perturbations of the end-effector and/or the movement's target. All simulations and evaluations were carried out on the same computer platform in MATLAB 2014b (Mathworks) using publicly available source code, trained modules, and the benchmark system[1] [28].

1) Dataset: The MG algorithms regenerated the human demonstrations $(N = 7)$ in different drawing tasks $(N = 30)$ (see Fig. 6). We first computed the optimal regeneration of the human trajectories without applying perturbations by directly solving the BVP problem (see Section III-C). Fig. 7 depicts the jerk and accuracy for different JA tradeoffs λ across all drawing tasks $(N = 30)$ and repetitions $(N = 7)$. Indeed, there is a tradeoff between the smoothness (jerk) and accuracy of the regenerated trajectories.

We next simulated perturbations for each of the measured human trajectories. Each regeneration consisted of perturbations according to different scenarios $(N = 4)$. The parameters of the perturbations were randomly drawn $(N = 100)$ from different distributions that pretended to generate movement uncertainties in natural motor tasks [28]. The evaluation metrics were calculated for each of the regenerated trajectories, and the median across demonstrations was stored for statistical analysis. The data consisted of 84 000 simulated trajectories $(N = 30 \times 7 \times 4 \times 100)$ for each MG algorithm.

2) Scenarios: The perturbations were organized according to four motor scenarios: *Push*, the end-effector was discretely pushed to a new location; *Target Displacement*, the final point of the movement was continuously perturbed during a selected time window; *Generalization*, the movement's onset location was changed; and *Continuous Push*, the end-effector was continuously pushed during a selected time window.

3) Metrics of Interest: We focused on metrics that evaluate human likeness: 1) the spatial and kinematic accuracy of the MG; and 2) the smoothness of the produced movements. All accuracy demands were calculated in a one-to-one fashion; a regenerated movement of a specific task had to be as close as possible to a specific demonstration of that task in the coordinate system of the human demonstration.

4) Performance: We computed the spatial and speed profile accuracy and the mean and maximal jerk in all motor scenarios (see Fig. 8). Averages and standard errors of performance metrics across perturbation parameters and repetitions were calculated. The two most compelling approaches in each scenario were compared using the Wilcoxon signed rank test: The RTJAMG generated trajectories ($p < 10^{-10}$) and speed profiles ($p < 10^{-20}$) were more accurate than TpGMM. The maximal

[1] http://pub.uni-bielefeld.de/data/2678439

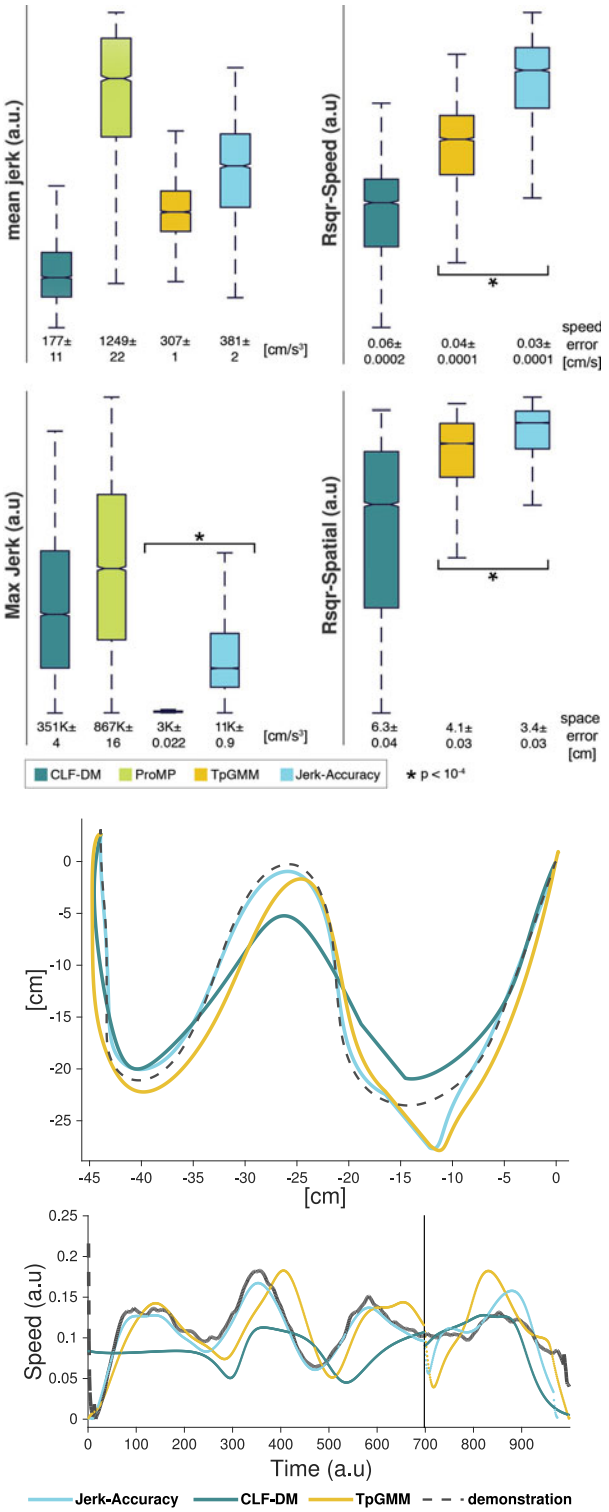

Fig. 8. (Top) Comparing the JA with other MG approaches using four metrics: spatial accuracy, speed accuracy, mean jerk, and max jerk [28]. The MG approaches are compared for each metric: the y-axis is scaled using a power transform defined by collapsing data across all methods. Numbers represent means $\pm$ SE. See Section V-C4 for a summary of the results. (Bottom) Real-time behavior of MG algorithms coping with a simulated discrete push perturbation. The spatial (top) and kinematic (bottom) accuracies are shown for JA, CLF-DM, and TpGMM MG algorithms. All three successfully generated the demonstrated trajectory under the discrete push perturbation scenario, but the performance of the JA and TpGMM was spatially more accurate, whereas the JA algorithm closely followed the demonstrated human speed profile.

jerk was larger in RTJAMG than in TpGMM ($p < 10^{-20}$). The mean jerk was smallest for TpGMM and CLF-DM. We collapsed the results across all scenarios and depicted the summary of all normalized distributions and the actual means and SEs in Fig. 8.

VI. Discussion

Here, optimization was combined with the principle of geometric invariance by choosing template curves as motion segments. A set of affine orbits has been used to update the original trajectory, and through adaptation, new trajectories have emerged, representing a tradeoff between cost minimization and accurate path following. We called our new formulation "the JA model."

We also investigated the mathematical conditions giving rise to maximally smooth movements. A characterizing equation (13) for path-constrained nth-order MSD optimization schemes was introduced. Complementary, local criteria that characterize smoothness maximization (15)–(17), as well as predictions of movement duration, were presented. Then, the affine invariance of the presented JA model (41) and different MSD optimization schemes was addressed.

End-effector execution was based on an optimal tradeoff between accuracy in following the motor plan and the smoothness of movement execution. We showed and benchmarked a closed-form solution for trajectory derivation satisfying this tradeoff when the trajectory describing the motor plan is maximally smooth (each coordinate is a polynomial in time). In this case, six affine orbits are superimposed as corrective terms added to the planned optimal polynomial trajectories. These constraints can optimally attract the system toward a desired behavior specified by the template. To regenerate arbitrarily complex trajectories under task-space perturbations, the RTJAMG converts in real-time portions of the planned movement to time polynomials and, using the state of the plant and the movement's target, linearly superimposes them with affine orbits, guarantying accuracy and maximal smoothness (the trajectory with the minimal jerk profile subject to a certain accuracy with respect to the planned trajectory).

The numerical algorithm for smooth trajectory regeneration (see Section III-C) can be beneficial to motion analysis in motor control studies. Human movements are prone to noise associated with motor commands at different levels of the motor hierarchy. The analysis of movement also suffers from the introduction of additional noise related to movement recording. Other studies have examined the nature of the noise associated with human movement, investigating different sources of noise either separately or in combination [11], [35], [52]. To reduce the noise caused by recording the produced trajectory, most motor control and robotic studies employ a model-free approach where trajectories are preprocessed based on an infinite impulse response and FIR filters. Here, we demonstrated that a model-based approach, which applies smoothness maximization, by applying template-based MSD minimization, can better denoise movement trajectories and allow inspecting finer movement properties (see Fig. 5). We suggest filtering

recorded trajectories by producing their maximally smooth updates constrained by the desired error between the recorded and produced trajectories (using the BVP formulation in Section III-C).

A. Geometrical Variance and Invariance

One important property of the smoothness index in (2) is the Euclidean invariance of the Lagrangian (i.e., unaffected by a rigid motion). This is consistent with the empirical observation of previous studies that the shape of the hand paths and velocity profiles of point-to-point movements do not strongly depend on the origin and orientation of the movement in task space. In a series of previous studies, it was shown that hand drawing and locomotion movements in the plane (i.e., here $d = 2$) follow the 2/3 power law, which is equivalent to moving at a constant equiaffine velocity [2], [25], which, up to a multiplicative factor, results from the unique parameterization that is invariant under affine transformation that also preserves areas. This geometrical description was then generalized to suggest that hand drawing and the center-of-mass trajectories during human locomotion emerge from the mixture of Euclidean and non-Euclidean (equiaffine and affine) geometries [2]. Due to the prevalence of such non-Euclidean geometries in human movement perception [19], [20], [53] and production [2], [25], [26], the invariance of smooth movements under such non-Euclidean geometries was suggested to indicate that the CNS may represent movements based on the mixture of these geometries. The L^2-norm of the jerk profile, however, is not invariant under non-Euclidean transformations.

The JA model presented in this paper is affine invariant in the sense discussed in Section IV. One of the perhaps unexpected properties of this model was a combination of affine invariant curves (affine orbits) with the planned movement via the superposition equation (39). This modeling further extends the already widely studied relationship between jerk minimization and affine invariance [2], [17], [25], [26]. Other explanations for the importance of affine invariance were discussed by Pham and Nakamura who suggested an algorithm for the correction of perturbed end-effector trajectories by efficiently applying affine transformations to preplanned trajectories.

A prominent law of movement associating movement kinematics and path geometry is the 2/3 power law (2/3PL), which states that speed of hand movements is proportional to the radius of curvature of the formed trajectory raised to the power of one third [14]. The close relationships between the minimum jerk model and the 2/3PL have been demonstrated and studied theoretically [4], [15]. It was also shown that the 2/3PL is equivalent to moving at a constant equiaffine speed [2], [25]. Later studies showed that the geometrical paths that minimize jerk, comply with the 2/3PL, and are invariant to equiaffine and full-affine transformations are parabolas [25], [26] and logarithmic spirals [45], [54], respectively. Based on invariant EL equations, Bright [54] derived logarithmic spirals combining the prediction of the minimum jerk model [4] with the requirement for the trajectories to have constant equiaffine, Euclidean, or affine velocities. These findings were generalized in [45], showing that orbits of affine geometry of planar curves provide movement segments that both minimize jerk and emerge from a mixture of trajectories that are invariant to Euclidean, equiaffine, and affine geometries [2]. We, therefore, hypothesized that affine orbits are potential movement primitives providing a succinct representation of human task-space trajectories. Here, we showed a direct use of affine orbits in optimal regeneration and updating of planned movements. In the case of a planned movement that is maximally smooth [3], the optimal recovery from perturbation is a superposition of the original plan (fifth-order time polynomial) and six affine orbits (log. spirals and hyperbolas).

The maximization of smoothness leads to simple geometrical requirements. The minimization of the n-order MSD functional imposes specific geometrical restrictions on optimal trajectories in the following way. Four motor tasks were considered here: point-to-point movements required to satisfy boundary conditions only at the end-points ("unconstrained"), via-point movements, path-constrained, and smooth movements required to track a geometrical template (the JA formulation). For all these cases, the control over the optimal movements is carried out in terms of the $2n-1$ and the $2n$-order time derivatives of position as follows.

For the unconstrained task, the $2n$-order time derivative of position must vanish everywhere. For the via-point task, the $2n$-order time derivative of position vanishes everywhere except at the via-point, where the normal to the path is coaligned with the vector resulting from the difference between the constant $(2n-1)$-order time derivatives of position before and after the via-point. For the path-constrained task, the direction of the movement must be perpendicular to the $2n$-order time derivative. Finally, for a smooth movement guided by a geometrical template, the direction of the "error" vector, namely, the vector representing the time-dependent difference between the produced and the template trajectories, must be coaligned and proportional to the $2n$-order time derivative of the produced trajectory.

These theoretical accounts suggest that achieving highly smooth MG requires careful control over specific high-order time derivatives. This "geometrical control" can simplify the control policy dictating the optimal production of the trajectories. Moreover, these geometrical criteria can be utilized for the segmentation of complex trajectories.

B. Predictability and Representation

We also showed how to locally derive distinctive and time-independent quantities from optimally smooth trajectories—these were referred to as "constants of motions." One example where this calculation proved useful was the derivation of the total duration from the constant of motion D_3 [see (15), (16), and (23)]. This calculation allows one to predict the duration of an ongoing smooth movement[55], irrespective of the existence of motor requirements such as the need to pass through via-points or to follow a path.

Finally, it still remains to assess the proposed real-time MG algorithm in a robotic system, as well as dealing with kinodynamic constraints [56].

APPENDIX A
REFORMULATING THE CONSTRAINED MINIMUM JERK

We minimize the MSD

$$I(s) = \int_0^T \left| \frac{d^n}{dt^n} \boldsymbol{r}(s) \right|^2 dt \tag{42}$$

for all possible real-valued monotonous functions $s(t)$ such that $\boldsymbol{r}(s) \in \mathbb{R}^2$ is the arclength parameterization of a prescribed path $\boldsymbol{r}$. For $n = 3$, this was termed the path constrained minimum jerk model [4]. Let $G(x, y)$ be the distance function of points $(x, y) \in \mathbb{R}^2$ from the path $r(s)$. Then, the path is defined by the implicit function

$$G(x, y) = 0.$$

A functional J of the form $J(q) = \int_{t_0}^{t_1} L(t, \boldsymbol{q}, \dot{\boldsymbol{q}}, \ddot{\boldsymbol{q}}, \dddot{\boldsymbol{q}}) dt$ has a continuously differentiable extremum at the generalized coordinate $\boldsymbol{q}(t)$ subject to the constraint $g(t, \boldsymbol{q}) = 0$ only if there exists a real-valued function $\lambda(t)$ such that $\boldsymbol{q}$ satisfies the EL equation $\sum_k (-1)^k \frac{d^k}{dt^k} \frac{\partial F}{\partial q_i^{(k)}} = 0$ for $F = L - \lambda(t) g$. Here, k enumerates the generalized task-space coordinates. In our case, $g(t, \boldsymbol{q}) = G(x, y) = 0$ and $L = {x^{(k)}}^2 + {y^{(k)}}^2$. Hence, the EL equations of (42) are

$$\begin{aligned} \frac{d^n}{dt^n} \frac{\partial L}{\partial x^{(k)}} - \lambda(t) \frac{\partial G}{\partial x} &= 0 \\ \frac{d^n}{dt^n} \frac{\partial L}{\partial y^{(k)}} - \lambda(t) \frac{\partial G}{\partial y} &= 0. \end{aligned}$$

Therefore

$$\boldsymbol{r}^{(2n)} \cdot \dot{\boldsymbol{r}} = 0 \tag{43}$$

is a necessary condition for minimizing the MSD along a path $\boldsymbol{r}(s)$. For the constrained minimum jerk model, the sixth-order time derivative of the trajectory must be perpendicular to the tangent to the path.

APPENDIX B
LOCAL CHARACTERIZATION OF JERK-MINIMIZING VIA-POINT TRAJECTORIES

For a minimal jerk trajectory, the derivatives at the via-point are continuous up to the fourth order [3]

$$\begin{aligned} &\forall t \in \Omega_- \\ &2\boldsymbol{r}^{(1)}(t) \cdot \boldsymbol{r}_-{}^{(5)}(t) - 2\boldsymbol{r}^{(2)}(t) \cdot \boldsymbol{r}^{(4)}(t) + \boldsymbol{r}^{(3)}(t) \cdot \boldsymbol{r}^{(3)}(t) = D_3^- \\ &\forall t \in \Omega_+ \\ &2\boldsymbol{r}^{(1)}(t) \cdot \boldsymbol{r}_+{}^{(5)}(t) - 2\boldsymbol{r}^{(2)}(t) \cdot \boldsymbol{r}^{(4)}(t) + \boldsymbol{r}^{(3)}(t) \cdot \boldsymbol{r}^{(3)}(t) = D_3^+ \end{aligned} \tag{44}$$

where Ω_- and Ω_+ are the time intervals before and after (and including) the via-point, and $\boldsymbol{r}_-{}^{(5)}$ and $\boldsymbol{r}_+{}^{(5)}$ are the fifth-order right and left time derivatives, before and after the via-point, respectively. The difference between the constants $D_3^+ - D_3^-$ can be directly calculated from (44). In particular, the difference $D_3^+ - D_3^-$ is expanded at the via-point:

$$\text{for } t \in \Omega_- \cap \Omega_+ \tag{45}$$
$$D_3^+ - D_3^- = 2\boldsymbol{r}^{(1)}(t) \cdot \left(\boldsymbol{r}_+{}^{(5)}(t) - \boldsymbol{r}_-{}^{(5)}(t) \right).$$

Due to (9) (proved in [3]), the inner product vanishes

$$2\boldsymbol{r}^{(1)}(t) \cdot \left(\boldsymbol{r}_+{}^{(5)}(t) - \boldsymbol{r}_-{}^{(5)}(t) \right) = 0. \tag{46}$$

Hence, $D_3^+ - D_3^- = 0$. This proves that for the smoothness maximization of a motor task with multiple via-points, all constants of motion D_3^i defined for each individual optimal segment are equal to one another, as required.

APPENDIX C
DERIVING THE TOTAL COST A_n FOR REST-TO-REST MOVEMENTS

For rest-to-rest movements in 3-D task space, the minimization of the n-order MSD cost function yields a trajectory $\boldsymbol{x}(t)$, whose coordinates $(x_1(t), x_2(t), x_3(t))$ are time polynomials of degree $2n - 1$, as in (4). Without loss of generality, we assume that the motion starts at the origin and that at $t = T$ $x_1(T) = L$ and $x_2(T) = x_3(T) = 0$ for some prescribed distance L. The rest-to-rest condition imposes that $\frac{d^k}{dt^k} x_i(t) = 0$ for $t \in \{0, T\}$, $k = 1, 2, \ldots, n-1$ and $i = 1, 2, 3$. In particular, $x_2(t) = x_3(t) = 0$ for all t. Let $\boldsymbol{a_n}$ be a generalized time vector $\boldsymbol{a_n}(t) = [1, t, t^2, \ldots, t^{2n-1}]$, and the coordinates of the vector $\boldsymbol{a} \in \mathbb{R}^{2n}$ are the polynomial coefficients such that $x_1(t) = \boldsymbol{a}\boldsymbol{a_n}^\tau$ satisfies the rest-to-rest boundary conditions. The vector $\boldsymbol{a}$ can then be solved linearly from the boundary conditions:

$$\begin{bmatrix} a_n(0) \\ \dot{a_n}(0) \\ \vdots \\ \frac{d^{n-1}}{dt^{n-1}} a_n(0) \\ a_n(0) a_n(T) \\ \dot{a_n}(T) \\ \vdots \\ \frac{d^{n-1}}{dt^{n-1}} a_n(T) \end{bmatrix} \cdot \boldsymbol{a} = \begin{bmatrix} 0 \\ 0 \\ \vdots \\ 0 \\ L \\ 0 \\ \vdots \\ 0 \end{bmatrix}.$$

We denote the RHS by $\boldsymbol{b} = [0, \ldots 0, L, 0, \ldots, 0]$ and the first term on the left-hand side by M. The coefficient vector $\boldsymbol{a}$ is given by $\boldsymbol{a} = M^{-1}\boldsymbol{b}$. The trajectory $x(t)$ then has the form

$$x_1(t) = L \sum_{k=1}^{2n-1} f_n(k) \, (t/T)^k$$

and $\frac{d^n}{dt^n}x_1(t) = L\sum_{k=1}^{2n-1} g_n(k)t^{k-n}/T^k$, where the functions f_n and g_n do not depend on L and T. Therefore

$$\int \left|\frac{d^n}{dt^n}x_1(t)\right|^2 dt = L^2 \sum_{k=1}^{2n-1} h_n(k)t^{k-2n+1}/T^k$$

and

$$\int_0^T \left|\frac{d^n}{dt^n}\boldsymbol{x}(t)\right|^2 dt = \bar{h}_n \frac{L^2}{T^{2n-1}}$$

where $= \bar{h}_n = \sum_{k=1}^{2n-1} h_n(k)$ is a function of n, as required.

ACKNOWLEDGMENT

The authors would like to thank M. Titon and M. Karklinsky for fruitful discussions.

REFERENCES

[1] I. L. Kurtzer, J. A. Pruszynski, and S. H. Scott, "Long-latency reflexes of the human arm reflect an internal model of limb dynamics," *Curr. Biol.*, vol. 18, no. 6, pp. 449–453, 2008.

[2] D. Bennequin, R. Fuchs, A. Berthoz, and T. Flash, "Movement timing and invariance arise from several geometries," *PLoS Comput. Biol.*, vol. 5, no. 7, p. e1000426, 2009.

[3] T. Flash and N. Hogan, "The coordination of arm movements: An experimentally confirmed mathematical model," *J. Neurosci.*, vol. 5, no. 7, pp. 1688–1703, 1985.

[4] E. Todorov and M. I. Jordan, "Smoothness maximization along a predefined path accurately predicts the speed profiles of complex arm movements," *J. Neurophysiol.*, vol. 80, pp. 696–714, 1998.

[5] B. Rohrer, "Movement smoothness changes during stroke recovery," *J. Neurosci.*, vol. 22, no. 18, pp. 8297–8304, 2002.

[6] S. Ben-Itzhak and A. Karniel, "Minimum acceleration criterion with constraints implies bang-bang control as an underlying principle for optimal trajectories of arm reaching movements," *Neural Comput.*, vol. 20, no. 3, pp. 779–812, 2008.

[7] Q.-C. Pham, H. Hicheur, G. Arechavaleta, J.-P. Laumond, and A. Berthoz, "The formation of trajectories during goal-oriented locomotion in humans. ii. a maximum smoothness model," *Eur. J. Neurosci.*, vol. 26, no. 8, pp. 2391–2403, 2007.

[8] E. Guigon, P. Baraduc, and M. Desmurget, "Computational motor control: Redundancy and invariance," *J. Neurophysiol.*, vol. 97, no. 1, pp. 331–347, 2007.

[9] A. Biess, D. G. Liebermann, and T. Flash, "A computational model for redundant human three-dimensional pointing movements: Integration of independent spatial and temporal motor plans simplifies movement dynamics," *J. Neurosci.*, vol. 27, no. 48, pp. 13045–13064, 2007.

[10] Y. Uno, M. Kawato, and R. Suzuki, "Formation and control of optimal trajectory in human multijoint arm movement," *Biol. Cybern.*, vol. 61, no. 2, pp. 89–101, 1989.

[11] C. M. Harris and D. M. Wolpert, "Signal-dependent noise determines motor planning," *Nature*, vol. 394, no. 6695, pp. 780–784, 1998.

[12] E. Todorov and M. I. Jordan, "Optimal feedback control as a theory of motor coordination," *Nature Neurosci.*, vol. 5, no. 11, pp. 1226–1235, 2002.

[13] W. Abend, E. Bizzi, and P. Morasso, "Human arm trajectory formation," *Brain: J. Neurol.*, vol. 105, no. Pt 2, pp. 331–348, 1982.

[14] F. Lacquaniti, C. Terzuolo, and P. Viviani, "The law relating kinematic and figural aspects of drawing movements," *Acta Psychol.*, vol. 54, pp. 115–130, 1983.

[15] M. J. Richardson and T. Flash, "Comparing smooth arm movements with the two-thirds power law and the related segmented-control hypothesis," *J. Neurosci.*, vol. 22, no. 18, pp. 8201–8211, 2002.

[16] D. Endres, Y. Meirovitch, T. Flash, and M. A. Giese, "Segmenting sign language into motor primitives with Bayesian binning," *Frontiers Comput. Neurosci.*, vol. 7, p. 68, 2013.

[17] D. Huh and T. J. Sejnowski, "Spectrum of power laws for curved hand movements," *Proc. Natl. Acad. Sci.*, vol. 112, pp. E3950–E3958, 2015.

[18] D. M. Wolpert, Z. Ghahramani, and M. I. Jordan, "An internal model for sensorimotor integration," *Science*, vol. 269, no. 5232, pp. 1880–1882, 1995.

[19] E. Dayan, A. Casile, N. Levit-Binnun, M. A. Giese, T. Hendler, and T. Flash, "Neural representations of kinematic laws of motion: evidence for action-perception coupling," *Proc. Nat. Acad. Sci. USA*, vol. 104, no. 51, pp. 20582–20587, Dec. 2007.

[20] Y. Meirovitch, H. Harris, E. Dayan, A. Arieli, and T. Flash, "Alpha and beta band event-related desynchronization reflects kinematic regularities," *J. Neurosci.*, vol. 35, no. 4, pp. 1627–1637, 2015.

[21] U. Pattacini, F. Nori, L. Natale, G. Metta, and G. Sandini, "An experimental evaluation of a novel minimum-jerk cartesian controller for humanoid robots," in *Proc. IEEE/RSJ Int. Conf. Intell. Robots Syst.*, 2010, pp. 1668–1674.

[22] K. Mombaur, J.-P. Laumond, and E. Yoshida, "An optimal control model unifying holonomic and nonholonomic walking," in *Proc. 8th IEEE-RAS Int. Conf. Humanoid Robots*, 2008, pp. 646–653.

[23] F. Amirabdollahian, R. Loureiro, and W. Harwin, "Minimum jerk trajectory control for rehabilitation and haptic applications," in *Proc. IEEE Int. Conf. Robot. Autom.*, 2002, vol. 4, pp. 3380–3385.

[24] K. Dautenhahn, S. Woods, C. Kaouri, M. L. Walters, K. L. Koay, and I. Werry, "What is a robot companion-friend, assistant or butler?" in *Proc. IEEE/RSJ Int. Conf. Intell. Robots Syst.*, 2005, pp. 1192–1197.

[25] A. Handzel, A. and T. Flash, "Geometric methods in the study of human motor control," *Cogn. Stud.*, vol. 6, no. 3, pp. 309–321, Sep. 1999.

[26] F. Polyakov, E. Stark, R. Drori, M. Abeles, and T. Flash, "Parabolic movement primitives and cortical states: Merging optimality with geometric invariance," *Biol. Cybern.*, vol. 100, no. 2, pp. 159–184, 2009.

[27] Q.-C. Pham and Y. Nakamura, "A new trajectory deformation algorithm based on affine transformations," *IEEE Trans. Robot.*, vol. 31, no. 4, pp. 1054–1063, Aug. 2015.

[28] A. Lemme, Y. Meirovitch, S. M. Khansari-Zadeh, T. Flash, A. Billard, and J. J. Steil, "Open-source benchmarking for learned reaching motion generation in robotics," *Paladyn, J. Behav. Robot.*, vol. 6, pp. 30–41, 2015.

[29] A. J. Ijspeert, J. Nakanishi, and S. Schaal, "Movement imitation with nonlinear dynamical systems in humanoid robots," in *Proc. IEEE Int. Conf. Robot. Autom.*, 2002, vol. 2, pp. 1398–1403.

[30] T. Kulvicius, K. Ning, M. Tamosiunaite, and F. Worgotter, "Joining movement sequences: Modified dynamic movement primitives for robotics applications exemplified on handwriting," *IEEE Trans. Robot.*, vol. 28, no. 1, pp. 145–157, Feb. 2012.

[31] T. Flash and B. Hochner, "Motor primitives in vertebrates and invertebrates," *Curr. Opin. Neurobiol.*, vol. 15, no. 6, pp. 660–666, 2005.

[32] S. Fleury, P. Soueres, J.-P. Laumond, and R. Chatila, "Primitives for smoothing mobile robot trajectories," *IEEE Trans. Robot. Autom.*, vol. 11, no. 3, pp. 441–448, Jun. 1995.

[33] P. M. Fitts, "The information capacity of the human motor system in controlling the amplitude of movement," *J. Exp. Psychol.*, vol. 47, pp. 381–391, 1954.

[34] N. Hogan, "An organizing principle for a class of voluntary movements," *J. Neurosci.*, vol. 4, no. 11, pp. 2745–2754, 1984.

[35] C. M. Harris, "On the optimal control of behaviour: A stochastic perspective," *J. Neurosci. Methods*, vol. 83, no. 1, pp. 73–88, 1998.

[36] M. Svinin, I. Goncharenko, Z.-W. Luo, and S. Hosoe, "Reaching movements in dynamic environments: How do we move flexible objects?" *IEEE Trans. Robot.*, vol. 22, no. 4, pp. 724–739, Aug. 2006.

[37] M. M. Svinin, I. A. Goncharenko, S. Hosoe, and Y. Osada, *Optimality Principles and Motion Planning of Human-Like Reaching Movements*. Rijeka, Croatia: InTech, 2010.

[38] F. Polyakov, "Motion primitives and invariants in monkey scribbling movements: Analysis and mathematical modeling of movement kinematics and neural activities," Dept. Comput. Sci. and App. Math., Ph.D. dissertation, Weizmann Inst. Sci., Rehovot, Israel, 2006.

[39] D. Huh, "Rethinking optimal control of human movements," Comput. Neurobio. Lab., Ph.D. dissertation, Salk Institute, Univ. California, San Diego, CA, USA, 2012.

[40] K. Goldberg, S. Faridani, and R. Alterovitz, "Two large open-access datasets for fitts? Law of human motion and a succinct derivation of the square-root variant," *IEEE Trans. Human-Mach. Syst.*, vol. 45, no. 1, pp. 62–73, Feb. 2015.

[41] C. M. Harris and D. M. Wolpert, "The main sequence of saccades optimizes speed-accuracy trade-off," *Biol. cybern.*, vol. 95, no. 1, pp. 21–29, 2006.

[42] D. E. Meyer, R. A. Abrams, S. Kornblum, C. E. Wright, and J. Keith Smith, "Optimality in human motor performance: Ideal control of rapid aimed movements." *Psychol. rev.*, vol. 95, no. 3, p. 340, 1988.
[43] K. Novak, L. Miller, and J. Houk, "The use of overlapping submovements in the control of rapid hand movements," *Exp. Brain Res.*, vol. 144, no. 3, pp. 351–364, 2002.
[44] H. Turnbull, "The matrix square and cube roots of unity," *J. London Math. Soc.*, vol. 1, no. 4, pp. 242–244, 1927.
[45] Y. Meirovitch, "Movement decomposition and compositionality based on geometric and kinematic principles," Dept. Comput. Sci. and App. Math., Ph.D. dissertation, Weizmann Inst. Sci., Rehovot, Israel, 2014.
[46] L. F. Shampine, J. Kierzenka, and M. W. Reichelt, "Solving boundary value problems for ordinary differential equations in MATLAB with BVP4C," *Tutorial Notes*, 2000.
[47] Q.-C. Pham and Y. Nakamura, "Affine trajectory deformation for redundant manipulators," in *Proc. Robot.: Sci. Syst. Conf.*, 2012, p. 504.
[48] A. Lemme, K. Neumann, F. R. Reinhart, and J. J. Steil, "Neural learning of vector fields for encoding stable dynamical systems," *Neurocomput.*, vol. 141, pp. 3–14, 2014.
[49] S. Calinon, T. Alizadeh, and D. G. Caldwell, "On improving the extrapolation capability of task-parameterized movement models," in *Proc. IEEE/RSJ Int. Conf. Intell. Robots Syst.*, 2013, pp. 610–616.
[50] S. Khansari-Zadeh and A. Billard, "Learning stable nonlinear dynamical systems with Gaussian mixture models," *IEEE Trans. Robot.*, vol. 27, no. 5, pp. 943–957, Oct. 2011.
[51] A. Paraschos, C. Daniel, J. Peters, and G. Neumann, "Probabilistic movement primitives," in *Proc. Adv. Neural Inf. Process. Syst. Conf.*, 2013, pp. 2616–2624.
[52] E. Todorov, "Stochastic optimal control and estimation methods adapted to the noise characteristics of the sensorimotor system," *Neural Comput.*, vol. 17, no. 5, pp. 1084–1108, 2005.
[53] N. Levit-Binnun, E. Schechtman, and T. Flash, "On the similarities between the perception and production of elliptical trajectories," *Exp. Brain Res.*, vol. 172, no. 4, pp. 533–555, 2006.
[54] I. Bright, "Motion planning through optimization," Dept. Math. M.S thesis, Weizmann Inst. Sci., Rehovot, Israel, 2007.
[55] H. Tanaka, J. W. Krakauer, and N. Qian, "An optimization principle for determining movement duration," *J. Neurophysiol.*, vol. 95, no. 6, pp. 3875–3886, 2006.
[56] Q.-C. Pham, S. Caron, and Y. Nakamura, "Kinodynamic planning in the configuration space via admissible velocity propagation," presented at the *Robot.: Sci. Syst. Conf.*, Berlin, Germany, 2013.

Yaron Meirovitch received the B.Sc. (Hons.) degree in computer science from Tel-Hai College, Upper Galilee, Israel, in 2003, and the M.Sc. and Ph.D. degrees in computer science and applied mathematics from the Weizmann Institute of Science, Rehovot, Israel, in 2006 and 2014, respectively, where he was supervised by Prof. T. Flash.

In his Ph.D., he investigated principles underlying human movement production and perception, using tools from differential geometry of curves, invariance theory, and optimization. Since 2015, he has been with the Computer Science and Artificial Intelligence Laboratory, Massachusetts Institute of Technology (MIT), Cambridge, MA, USA, working on the big data challenge of connectomics with Dr. N. Shavit (MIT) and Dr. J. Lichtman (Harvard).

Daniel Bennequin was born in 1952. He graduated from École Normale Supérieure, Paris, France. He received the Ph.D. degree (with A. Chenciner) in contact geometry from Paris Diderot University, Paris, in 1982.

He was a Professor with the University of Strasbourg, Strasbourg, France. He is currently a Professor with Paris Diderot University, Paris, France, and a member of the IMJ. During the 1980s, he was the initiator of contact topology with Y. Eliashberg. During the 1990s, he worked on integrable systems and geometry of mathematical physics. Since 2000, he has been working in neurosciences (mainly with A. Berthoz, C-d-F, and T. Flash, Weizmann Institute of Science, Rehovot, Israel); he made contributions to the study of human movement duration, vestibular information flow, and gaze functions during locomotion. His most recent publications are on information topology (with P. Baudot) and psychic pain (with M. Bompard-Porte).

Tamar Flash was born in Ramat Gan, Israel. She received the B.Sc. degree in physics in 1972 and the M.Sc. degree in 1976, both from Tel Aviv University, Tel Aviv, Israel. In 1978, she joined the Ph.D. program in medical physics and medical engineering, run by the Harvard-MIT Division of Health Sciences and Technology, and received the Ph.D. degree from the Massachusetts Institute of Technology (MIT), Cambridge, MA, USA, in 1983. She continued her postdoctoral studies with the Department of Brain and Cognitive Science and the Artificial Intelligence Laboratory, MIT, until 1985, when she returned to Israel to join the Department of Computer Science and Applied Mathematics, Weizmann Institute of Science, Rehovot, Israel, where she became an Associate Professor in 1991 and Full Professor in 1998. She was a visiting scientist with MIT (1991–1992), and the College de France, Paris, France (2002–2003), University of California, Berkeley, Berkeley, California, USA (2015–2016), and a Fellow of the Radcliffe School of Advanced Studies, Harvard University, Cambridge, MA, USA in 2012. During 2004 to 2006, she served as chair of the Department of Computer Science and Applied Mathematics. She is the incumbent of the Dr. Hymie Moross Professorial Chair. Her research interests include computational neuroscience, motor control, and robotics.